Graduate Theses, Dissertations, and Problem Reports

2018

Shale Characterization and Size-effect study using Scanning Electron Microscopy and X-Ray Diffraction

Debashis Das
West Virginia University, debashis520@gmail.com

Shale Characterization and Size-effect study using Scanning Electron Microscopy and X-Ray Diffraction

Debashis Das

Thesis submitted to the

Benjamin M. Statler College of Engineering and Mineral Resources

at West Virginia University

in partial fulfillment of the requirements for the degree of

Master of Science

in

Mining Engineering

Brijes Mishra, Ph.D., Chair

Yi Luo, Ph.D., P.E.

Qingqing Huang, Ph.D., P.E.

Department of Mining Engineering

Morgantown, West Virginia

2018

Keywords: Size effect, Marcellus shale, XRD (X-Ray diffraction), SEM (Scanning Electron Microscopy), Grain size, Quartz content, Grain shape

ABSTRACT

Shale Characterization and Size-effect study using Scanning Electron Microscopy and X-Ray Diffraction

Debashis Das

Ground failure is a major contributor of the total fatalities in underground mines in the US. Underground coal mines in the Northern Appalachian region have weak roof rock mainly composed of shale and sandstone. Characterization of shale is indispensable for developing an effective ground control plan. However, this has not been done extensively. This thesis attempts to address this issue. It investigates the variation in mechanical properties of shale with variation in size. In addition, an attempt has been made to relate the strength of shale with its petrographic parameters. X-ray diffraction technique was used to estimate the compositional parameters like quartz content, calcite content and clay content. Similarly, scanning electron microscopy was used to image the rock sample at microscale and estimate grain properties such as grain size, grain shape and grain orientation. Statistical analysis was performed to identify the extent of correlation between these parameters and strength and size of sample. From the analysis, it was observed that there was a significant difference in the strength of the sample with variation in size. In addition, samples with high quartz and calcite content showed higher average strength. Grain parameters also played a major role in influencing the strength of the sample with samples having higher average grain size inclining to have lower strength. Grain shape when defined by aspect ratio correlated with the strength of shale with higher aspect ratio contributing to higher strength. Grain orientation did not have any impact on strength. Finally, this research will help in understanding the size effect phenomenon in mines by looking into shale rock at microscopic scale and analyzing its petrographic parameters.

ACKNOWLEDGEMENTS

like to thank Gunes Yakaboylu for helping me in developing the method for sample preparation for SEM.

Lastly, I would like to thank my parents and my brother for their encouragement and support during my study. Finally, I thank God for carrying me through all the joys and sorrows during my stay at WVU and making me a better person through each passing day.

TABLE OF CONTENTS

LIST OF FIGURES

LIST OF TABLES

Chapter 1: Introduction

1.1 Background

Pappas and Mark (2009) of MSHA (Mine Safety and Health Administration) investigated the groundfall incidents in US underground coal mines from 1999 to 2008. They found that these events resulted in 75 fatalities, 5,941 injuries and 13,774 non-injury roof falls. Mark, Pappas and Barczak (2009) found that ground falls are responsible for nearly 50% of the fatalities in underground bituminous coal mines in the US. Bajpayee, Pappas and Ellenberger (2014) gathered information from the reportable non-injury roof falls. They identified the geological factors contributing to roof falls, the relationship between bolt length and height of roof fall cavities and the distribution of roof fall in different mining regions in the US. For normalizing the data across different mines, they estimated the number of roof falls per 200,000 employee hours. They found that Northern West Virginia-Ohio-Maryland region experienced the highest roof fall rate followed by Illinois-Indiana and Western Kentucky regions. They also found that coal mines in the Illinois basin are particularly susceptible to roof falls. They also found that about 70% of the roof falls do not exceed two feet above the bolted horizon.

From the studies reviewed above, it is evident that roof falls continue to be a major problem in underground coal mines in the US. The coal mines in the northern Appalachian and Illinois basin are susceptible to roof falls. Due to the presence of weak laminations within shale or thinly interbedded sandstone and shale layers, also referred to as stack rock in the roof and high horizontal stress in the region, the mine roofs are exposed to cutter roof failure as proposed by Molinda (2003). Cutter roof is a compression failure which originates at the corners of the entry and propagates towards the roof, or begins in the roof and cuts downwards (Molinda & Mark).

Murphy (2016) stated that characterization of the roof rock is necessary for developing a proper ground control plan aiming towards a safe working environment. This thesis seeks to achieve an accurate characterization of roof rock. The goal is to understand the mechanical behavior of the shale rock and characterize the petrographic properties. The size effect in shale is also investigated in the thesis that will provide a clear understanding of the variation in strength of rock with change in size and can help in developing an effective roof support plan.

1.2 Objective

The objectives addressed in this thesis are discussed below:

- Effect of Size on strength of shale
- Causes for variation in strength of different sized shale samples by performing petrographic analysis:
    - Composition analysis by X-ray diffraction method
    - Grain parameter analysis by Scanning electron microscopy

1.3 Thesis organization

The thesis is divided into six chapters. A brief summary of the topics discussed in the six chapters is mentioned below:

Chapter 1:

Chapter 1 includes the background of the research. It explains the necessity of this research and its contribution to the mining industry. Another section details the objective of the research.

Chapter 2:

Chapter 2 summarizes the literature reviewed to develop the gaps in reported research and also develop a research plan. It mainly includes the review of published literature on size effect for coal, rocks such as sandstone and limestone and concrete. It also contains a review of the parameters to be studied for petrographic analysis and the instruments such as scanning electron microscope and X-ray diffraction used for quantitative analysis of those parameters.

Chapter 3:

Chapter 3 discusses the uniaxial compressive strength tests performed on specimens of different sizes. It details the test setup, input test parameters and post failure mode. It also contains a statistical analysis of the strength with size to understand whether the size of the specimen was a factor influencing its strength.

Chapter 4:

Chapter 4 includes X-ray diffraction analysis. It emphasizes on sample preparation, instrument set up and the results. XRD analysis gives a semi-quantitative estimate of the minerals present in the sample. The relationship between the minerals and the average strength of the different sized samples is investigated through XRD analysis

Chapter 5:

Chapter 5 deals with Scanning Electron Microscopy. It comprises of the sample preparation procedure which forms the mainstay of grain parameter analysis. It also discusses the image analysis procedure used for quantitative estimate of the grain parameters. Finally, analysis is performed to determine the contribution of these grain parameters to the strength of the samples.

Chapter 6:

Chapter 6 contains a summary of the results. It underlines the parameters affecting the strength of the rock. It also contains the limitations of the study and further research scope in this work.

In addition to the chapters discussed above, the thesis also contains two Appendices.

Appendix A describes the bulk XRD analysis method and explains how it is different from powdered XRD analysis.

Appendix B describes in detail the iterative process of SEM sample preparation to arrive at a method which gives the desired result.

Chapter 2: Literature review

The literature reviewed for the thesis is subdivided into the following categories:

- Size effect on strength of rock: To get a general overview of the major processes involved in size effect study, a thorough literature review was performed on materials such as coal, limestone, granite, concrete, sandstone. Similarly, other materials were extensively reviewed to find the relationship between their size and strength.

- Petrographic parameters and their estimation: The second section of the literature review discusses the petrographic parameters like quartz content, grain size, grain shape, grain interlocking and their correlation with strength. Finally, the basic principle of the instruments such as X-ray diffraction and scanning electron microscope was reviewed to quantify these parameters.

2.1. Size effect study literature:

2.1.1. Coal:

Bieniawski (1968) investigated the size effect in coal with numerous field studies. Different sized specimens were subjected to *in-situ* uniaxial compression tests. The effort involved large scale of testing of coal specimens of various dimensions as shown in Table 1. The specimens were prepared using coal saw. Load was applied on to the specimen using multiple hydraulic jacks. The deformation of the specimens was measured using displacement gauges.

Table 1. Dimensions of cubic specimen and their strength obtained from test (Bieniawski, 1968)

Cubic size (in.)	Number of tests	Strength (lbs./sq. in)	Deviation (lbs./sq. in.)
0.75	10	4,260	814
1	10	4,760	700
2	8	4,880	1,070
2.7	5	4,575	1,250
3	6	4,070	400
6	7	1,850	435
12	4	1,158	115
18	2	910	12
24	1	800	-

28	1	774	-
36	2	709	2
48	2	650	20
60	2	643.5	20

The plot between cube size coal specimen and strength is shown in Figure 1. The figure shows that when the specimen size is small then the strength is high and as the size increases the strength decreases. However, the effect on the strength remains constant after 60 inches.
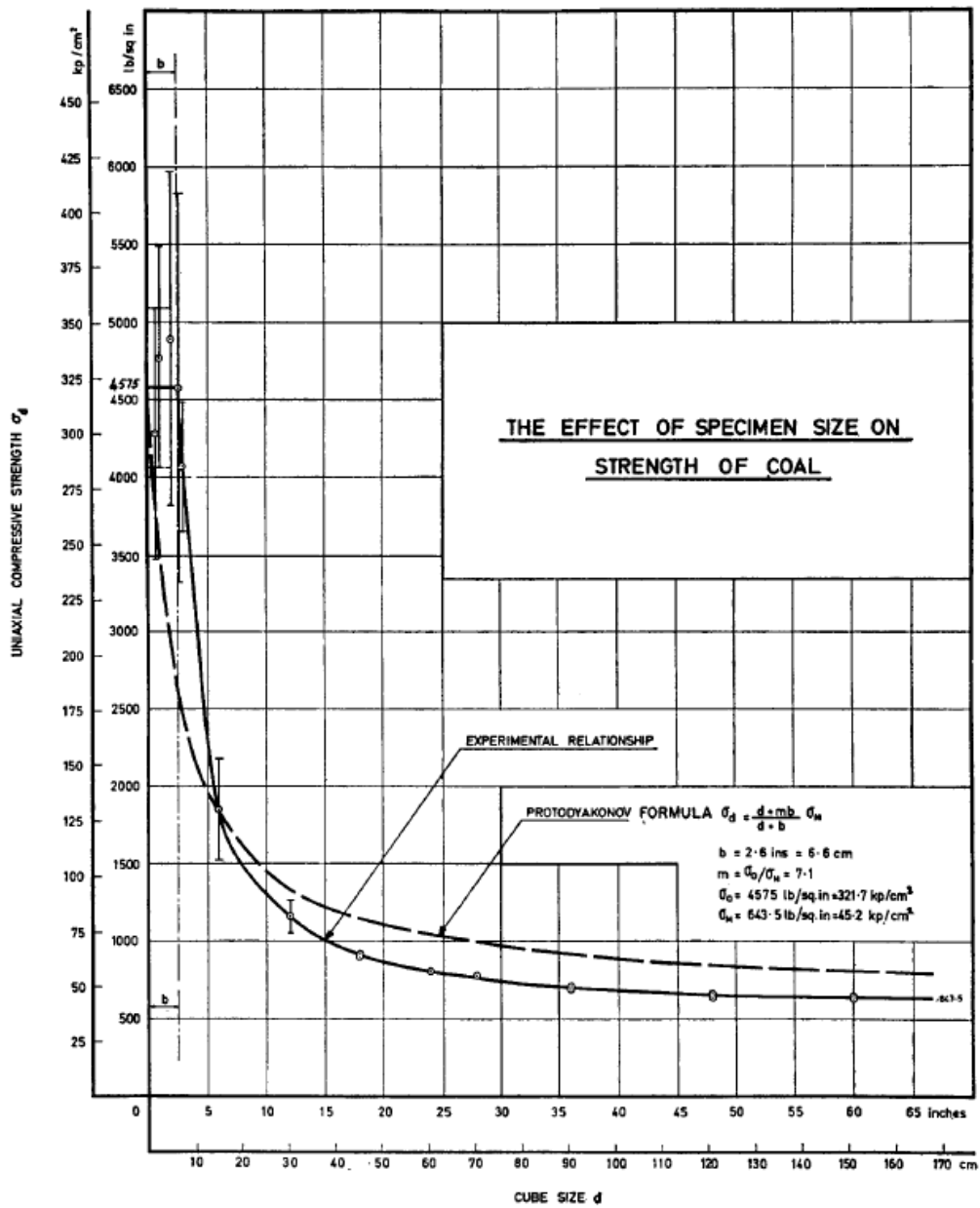
Figure 1. Effect of specimen size on the strength of coal (Bieniawski, 1968)

Skelly et al. (1977) conducted tests on core specimens with a range of diameters (1 to 12 in) and varying length over diameter ratio. The variation of UCS with diameter was expressed in the form of the following equation:

$$\sigma_1 = 2360(D)^{-0.21}(psi) \hspace{3cm} \text{Equation 1}$$

(D is expressed in inches)

The tests showed that the strength of coal sample decreases as the specimen size increases.

Gaddy (1956) proposed the strength equation for US coal and showed that the compressive strength of a cubical specimen decreases with increase in size of the specimen. The equation is:

$$S_c = \frac{K}{\sqrt{d}} \hspace{3cm} \text{Equation 2}$$

Where, S_c= compressive strength of cubical specimen (psi)

      K= a material constant

      d= edge length of the cubical coal specimen (inches)

Steart (1954) also independently studied the behavior of coal specimen with increasing size and proposed an inverse relationship.

Evans and Pomeroy (1958) conducted uniaxial compression tests on Deep Duffryn and Barnsley hard coal cubes and found that the compressive strength is exponentially related to the side length of cube which is expressed in the Equation 3: The plot shown in Figure 2 indicate that the strength of coal linearly decreases with increase in the side length of the cube.

$$Q = a^\beta \hspace{3cm} \text{Equation 3}$$

Where: Q = compressive strength (psi)

    a = side length of cube (inches)

    β = material constant
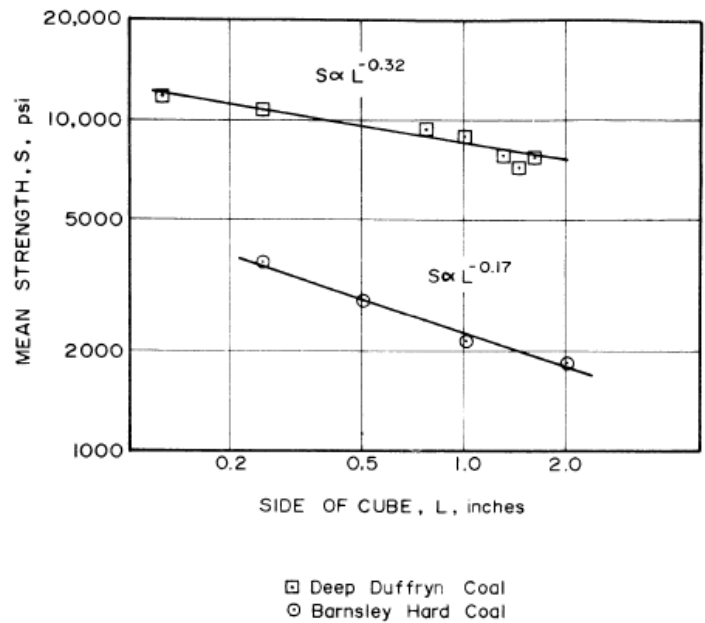
Figure 2. Relation between compressive strength and side length of coal cube specimens (Evans and Pomeroy, 1958)

Medhurst and Brown (1998) conducted triaxial tests on coal specimens of diameter 61, 101, 146 and 300 mm and found that the peak strength of the sample decreases with an increase in size at a fixed confining pressure.

Table 2. Influence of sample size on coal peak strength in triaxial test (Medhurst and Brown, 1998)

Confining Pressure (MPa)	Sample diameter (mm)	Number of samples	Mean (MPa)	Coefficient of variation (%)	ANOVA significance level α=0.05		
					F	F_{crit}	P-value
0.2	61	3	26.1	4.5	26.1	4.8	0.0007
	101	2	26.7	3.5			
	146	4	18.0	12.6			
	300	1	12.6	-			

7

2.1.2. Rock:

Bieniawski (1972) conducted UCS tests on norite cubes ranging in length from 0.5 inches to 8 inches. The strength of norite decreased when size increased from 0.5 inch to 5 inches. As shown in figure 3, the strength remained constant for additional increase in size of the cube.
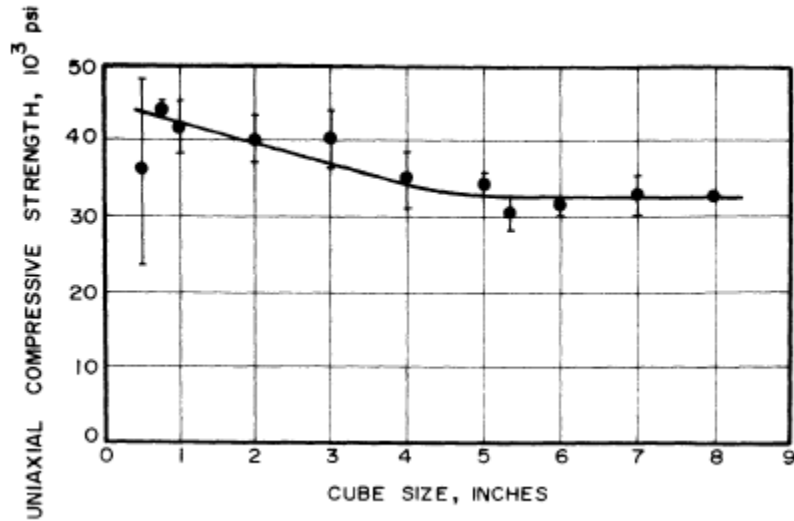
Figure 3. The effect of specimen size on the compressive strength of Norite (Bieniawski, 1972)

Hodgson and Cook (1970) conducted uniaxial compression tests on shale and quartzite specimen and found no pronounced size effect. In figure 4, it is observed that the strength of both shale and quartzite varied minimally with increase in the diameter of the specimen.
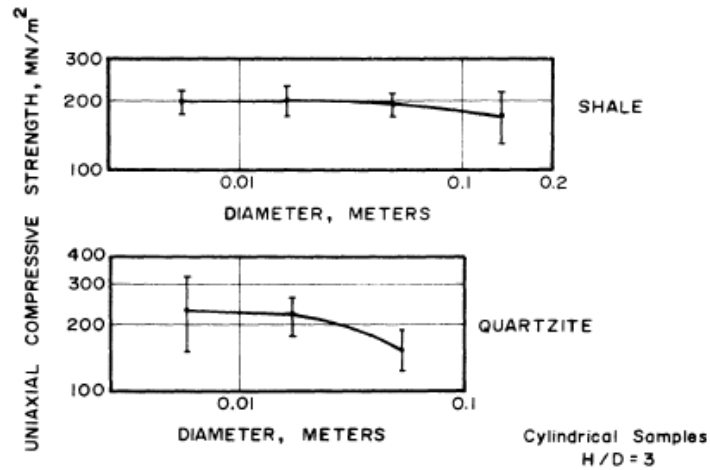
Figure 4. The influence of specimen size on the compressive strength of shale and quartzite (Hodgson and Cook, 1970)

8

Mogi (1962), by conducting experiments on marble found that the strength followed an expression as provided in Equation 4. The strength in the specimen decreased linearly with increase in the specimen's lateral dimension.

$$S = S_o L^r \qquad \qquad \text{Equation 4}$$

Where: S = compressive strength (kg/cm)

L = specimen dimensions (cm)

S_o, r = material constants
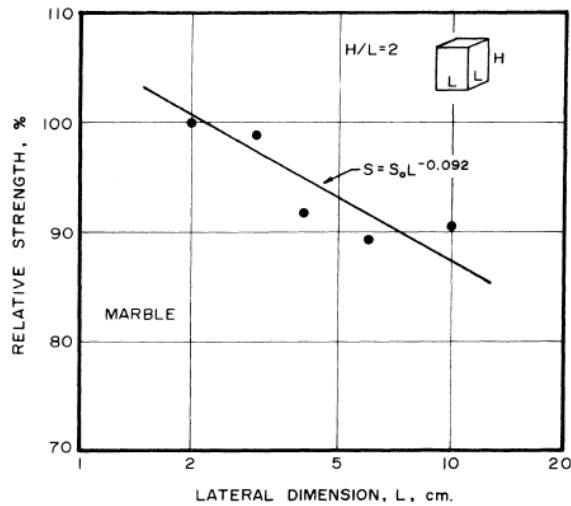
Figure 5. Relation between compressive strength and specimen dimensions (Mogi, 1962)

Hoskins and Horino (1969) conducted uniaxial compressive tests on cylindrical specimens (length/diameter = 2) of limestone, marble, sandstone and granite. It was observed that compressive strength decreased with increased size in granite. In other rocks, the general trend of decreasing strength with increasing sample size was not noticeable.

Pratt et al. (1972) conducted uniaxial compressive tests on quartz diorite in both laboratory and in-situ to determine the mechanical properties (Figure 6). Two types of laboratory specimens, triangular and cylindrical were tested in the laboratory. The length of triangular specimens varied from 4.5 to 12" whereas cylinders were 3.18 to 4.25" long. The length over diameter ratio was greater than or equal to 1.5. The test showed wide variation in strength for approximately 3 inches

9

in length. The strength decreased asymptotically, approaching a constant value for in-situ specimens greater than 3 feet in length.
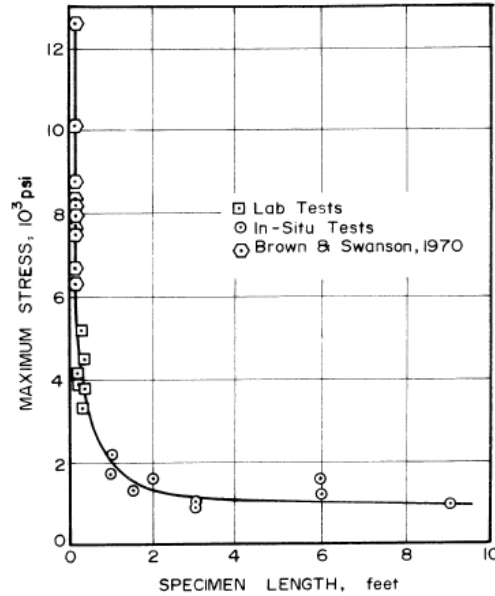
Figure 6. The influence of specimen size on strength in Quartz diorite (Pratt, Black, Brown and Brace, 1972)

2.1.3. Concrete:

Gonnerman (1925) showed for concrete cylinders that the variation in length from 0.5 to 4 times of the diameter caused the strength to decrease from 1.78 to 0.9 times the strength of cylinder with l/d (length/diameter) ratio equal to two. Blanks and McNamara (1935) showed that for concrete cylinders of different sizes, the strength decreased with increase in the size of the cylinder. Gyengo (1938) tested different sized cubes, prisms with variable slenderness, and cylinders. Comparison of 28-day compressive strengths of specimens with equal slenderness and ratio with size showed equal strength. Mogi (1962) found that the uniaxial strength of concrete followed the empirical relation:

$$S = S_o L^r \hspace{4cm} \text{Equation 5}$$

Where: S = uniaxial compressive strength (kg/cm)

L = specimen dimension (cm)

10

S_o and r = material constants (S_o = UCS as L → 0)
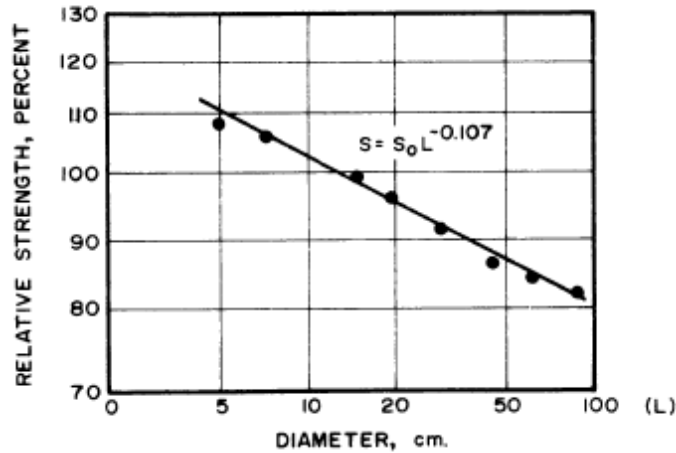
Figure 7. Relation between compressive strength and specimen dimensions (Mogi, 1962)

MacGregor (1994) studied the effect of specimen diameter on the compressive strength of concrete cores. They found that the compressive strength of the 2-inch diameter cores is more affected by the core length-to-diameter ratio than the 4-inch diameter. Tokyay and Ozdemir (1997) studied the specimen size and shape effects on the compressive strength of higher strength concrete (Figure 8). Different sized cylinders having constant length-to-diameter ratio (l/d) and different sized cubes and cylinders with varying l/d for 40, 60 and 75 MPa confining stress levels were tested. There was no significant variation of strength with change in cylinder diameter or cube size at a particular confining pressure (Figure 9). The compressive strength of the high strength concrete increased with an increase in confining pressure in both the cylinder and the cube.
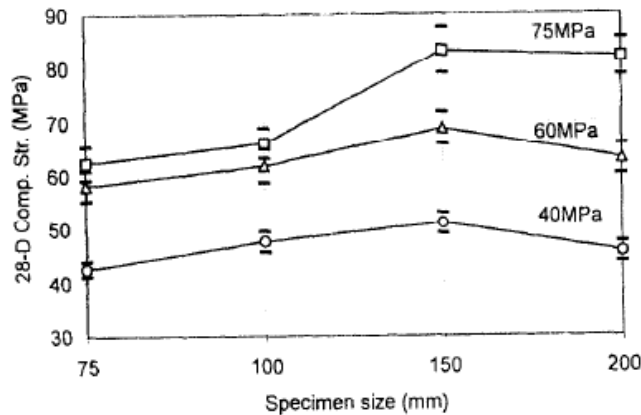
Figure 8. Average strength values and standard deviation from different sized cubes (Tokyay and Ozdemir, 1997)

11
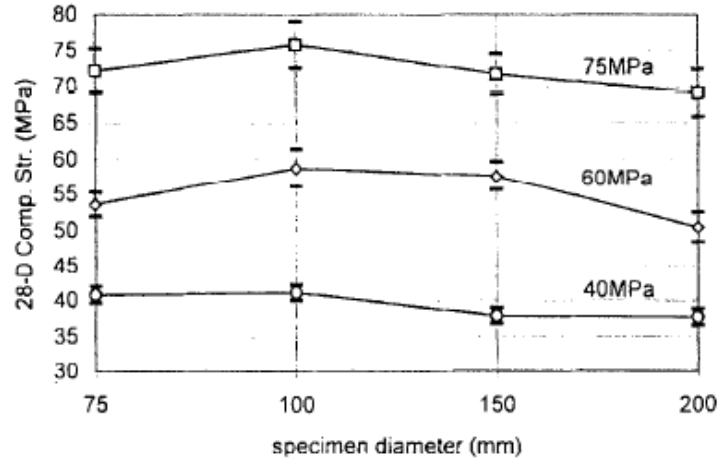
Figure 9. Avg. strength values and std. dev. Obtained from diff. sized cylinders with l/d=2 (Tokyay and Ozdemir, 1997)

2.1.4. Other materials:

Griffith (1920) conducted tensile tests on glass fibers and found the strength to decrease with increasing fiber diameter. Griffith mentioned that the test specimens were not produced under adequately controlled conditions but nevertheless the trend of decreasing stress with increasing size was evident (Figure 10).
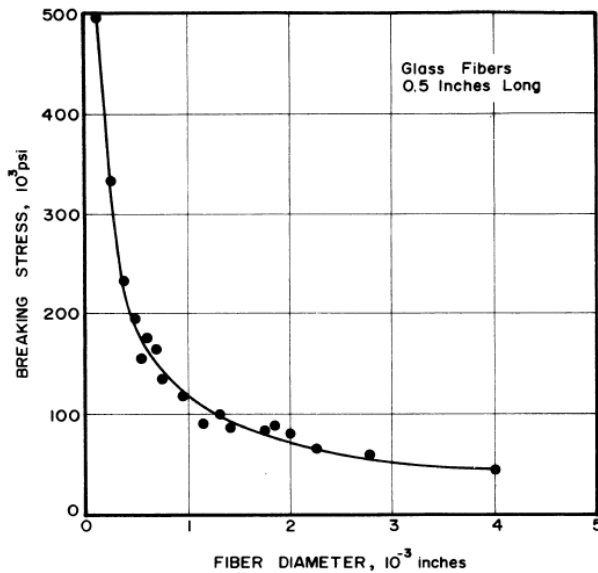
Figure 10. Size effect in glass fibers (Griffith, 1920)

2.1.5. Combined review by Hoek-Brown:

Hoek and Brown (1980) reviewed the size effect on strength mainly for igneous rocks. The uniaxial compressive strength for a 50 mm was normalized and compared against the different sized diameter of various rock types. It was found that the normalized UCS decreased with increase in the specimen diameter as shown in Figure 11. Based on the plot a relationship for the conversion of the result obtained for different diameter of the specimens is provided in equation 6.

$$\frac{UCS}{UCS_{D50}} = \left(\frac{50}{D}\right)^{0.18}$$
                                                                                              Equation 6

Where: UCS is the uniaxial compressive strength of the specimen

UCS_{D50} is the uniaxial compressive strength of 50 mm diameter specimen.

D is the diameter of the specimen in mm.
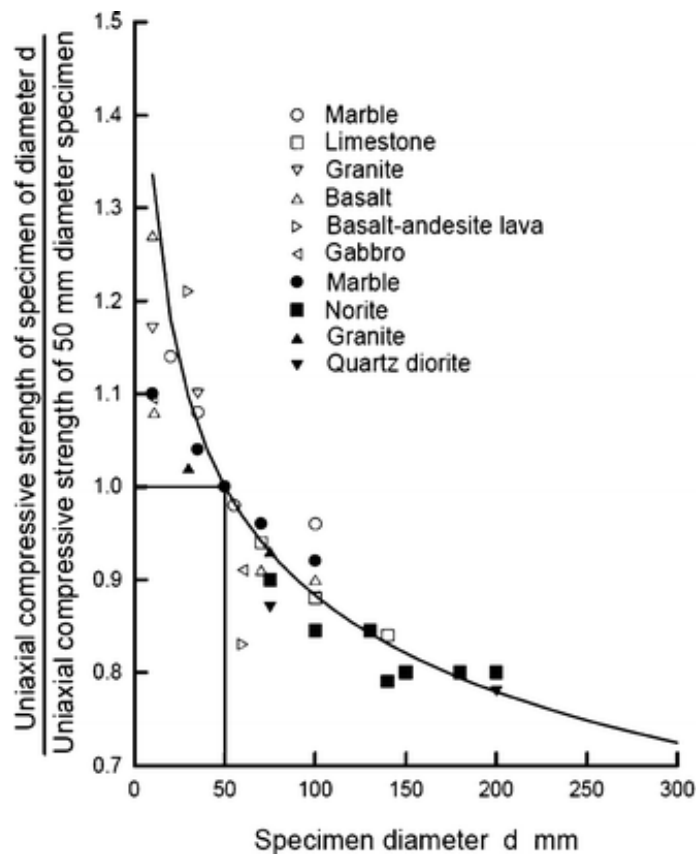
Figure 11. Influence of specimen size on strength of igneous rocks (Hoek and Brown, 1980)

13

Summary

- It is seen from the literature study that for coal, rock, concrete or glass, the strength decreases with increase in the size of the specimen. However, research also showed no correlation between strength and size. This observation stresses on the fact that rock is highly heterogeneous, and the strength obtained is also governed by local factors and geological variability in the region.

- The strength does not change beyond a critical size.

- Size effect has been studied with different specimen shapes such as cylindrical, cubical and prisms. The effect of increasing size on the strength is similar for all the cases

- Few literatures reported on size effect for coal measures roof rock and in particular on shale.

2.2. Microscopic Study

2.2.1. Petrographic Parameters:

Numerous reported research has shown the relationship between petrographic and mechanical properties of sandstone, however few have reported for coal measures roof rock. Phillipson (2008) discussed the variation of strength of coal measure roof rock with petrographic parameters. It is found that the quartz content of immediate roof shale does not appear to be related to rock strength. For the fine-grained specimens of immediate coal mine roof collected in this study, there is no correlation between the quartz content and the unconfined compressive strength. Surprisingly, there is no correlation between unconfined compressive strength and the percentage of sutured mica grain boundaries. Similarly, there is no correlation between grain size and compressive strength. These observations are generally at variance with the results reported for previous studies of sandstone. In this thesis, the aim is to investigate the change in petrographic properties with change in the size of the specimen, which additional leads to variation in strength. Following are the parameters which need to be studied under petrographic analysis. Majority of the literature reviewed is for sandstone.

2.2.1.1. Quartz Content:

Increase in quartz content increases the uniaxial compressive strength of sandstone (Smart, Rowlands and Isaac (1982), Gunsalles and Kulhaway (1984) and Shakoor and Bonelli (1991)).

However, uniaxial compressive strength was not found unaffected by quartz content Bell ((1978), Barbour, Atkinson, and Ko (1979) and Dobereiner and De Freitas (1986)).

2.2.1.2. Cement and matrix:

Clough, Sitar and Bachus (1981) and David, Menendez and Bernabe (1998) found that sandstone with higher cement content have higher strength than sandstone with lower cement content. Vutukuri, Lama and Saluja (1974) also found that the type of cement also affects sandstones' strength. Sandstones with silica or calcareous cement have higher strength than the ones with clay mineral content.

2.2.1.3. Grain size:

The effect of grain size on rock strength varies with the rock type being tested. Singh (1988) found that an increase in grain size results in a decrease in uniaxial compressive strength for greywacke while in other cases, there was no correlation between the grain size and strength (Shakoor and Bonelli (1991) and Palchik (1999)). In case of sandstone, fine grained sandstone exhibits higher strength as compared to coarse grained sandstone (Fahy and Guccione (1979) and Ulusay, Tureli and Ider (1999)).

2.2.1.4. Grain shape:

Grain shape exerts significant control on sandstone strength as evidenced by Taylor (1950), Spry (1976), Fahy and Guccione (1979) and Hawkins and McConnell (1990) and studies of sandstone by Fahy and Guccione (1979) indicated that sphericity was inversely correlated with compressive strength.

2.2.1.5. Grain interlocking:

Taylor (1950), Fahy and Guccione (1979) and Hawkins and McConnell (1990) recognized the influence of grain interlocking on sandstone strength. Taylor (1950) assigned weights to classifications of grain boundaries, such that the tangential contacts are weighted as 1× (1 times), long contacts were weighted as 2× (2 times), concavo-convex contacts were weighted as 3× (3 times) and sutured contacts were weighted as 4× (4 times). Howarth and Rowlands (1986) concluded that shear failure of crystals and crystal grains is resisted by interlocking grains. Shakoor

and Bonelli (1991) found that sandstone with higher percentage of sutured grain contacts exhibited higher values of compressive strength, tensile strength and Young's modulus.

2.2.1.6. Packing density:

Packing density is defined as the space in a specified area occupied by grains. Bell (1978) found that with an increase in packing density in sandstone increased the uniaxial compressive strength, tensile strength and Young's modulus.

2.2.1.7. Porosity:

Crack porosity plays a significant role in mechanical performance. In sedimentary rocks, all strength properties decrease with increase in porosity according to Price (1960), Smordinov, Motovilov and Volkov (1970) and Dube and Singh (1972). Price (1960) conducted investigations in coal measures rocks which showed that UCS decreased linearly with increase in porosity.

2.2.1.8. Micro-fractures:

Spry (1976), Tugrul and Zarif (1999), Prikryl (2001) and Edet (1992) found that the total rock strength in any rock is reduced by the presence of macroscopic, microscopic and sub-microscopic defects such as cavities, cracks, joints, foliations and veins.

2.2.2. Rock texture coefficient:

Howarth and Rowlands (1986) developed a parameter called texture coefficient which comprised of the contribution of grain shape, grain elongation, grain orientation and packing density of the rock. They found statistically significant correlation between texture coefficient and the strength of the rock. Hence, they concluded that texture coefficient can be utilized as a predictive tool for assessing rock mechanical performance. The formula can be written as:

$$TC = AW\left[\left(\frac{N_0}{N_0+N_1} \times \frac{1}{FF_0}\right) + \left(\frac{N_0}{N_0+N_1} \times AR_1 \times AF_1\right)\right] \qquad \text{Equation 7}$$

Where,

TC = Texture coefficient

AW = Area weighting (grain packing density)

N_0 = Number of grains with aspect ratio (maximum Feret's diameter or length to minimum Feret's diameter or breadth) less than 2.0

N_1 = Number of grains with aspect ratio greater than 2.0

FF_0 = Arithmetic mean of form factor of all N_0 grains

AR_1 = Arithmetic mean of aspect ratio of N_1 grains

AF_1 = Angle factor orientation which were computed for all N_1 grains

2.2.3. Instruments for microscopic study:

2.2.3.1. XRD (X-Ray diffraction) technique:

According to Dutrow and Clark (2017), X-ray diffraction technique is used for semi-quantitative analysis of the minerals present in the specimen. X-rays generated from a cathode ray tube are concentrated using a collimator and filtered to generate monochromatic rays using the screen (Figure 12). These rays are then allowed to penetrate the specimen. The specimen is generally powdered as it helps to identify the different phases of individual minerals present. In a crystalline sample, which has a defined structure, the incident X-rays undergo constructive or destructive interference when they interact with the atoms of the mineral. Constructive interference takes place when Bragg's law is satisfied ($n\lambda = 2d \sin \theta$). Bragg's law identifies the relationship between the wavelength of the incident monochromatic radiation and the lattice spacing of the mineral with which it interacts. The sample is scanned through 2θ angles and the diffracted X-rays are processed and counted. Every mineral has a unique set of d-spacing which translates to different peaks observed in the diffraction pattern which helps in identification of the mineral.
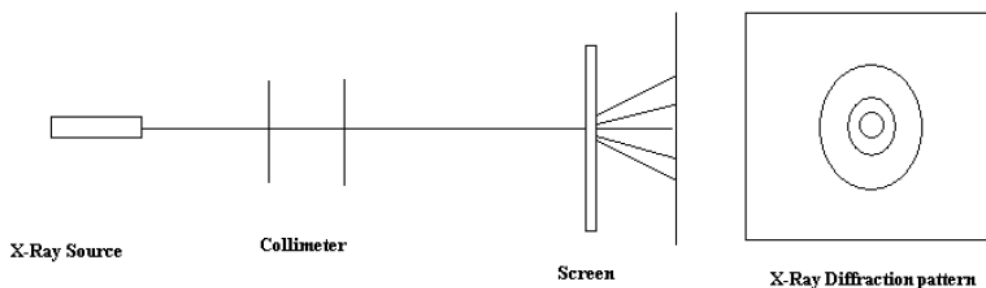
Figure 12. A schematic diagram of X-ray diffraction pattern (Gowariker, Viswanthan and Sreedhar, 1986)

17

2.2.3.2. SEM (Scanning Electron Microscopy):

In a scanning electron microscope, incident electrons from the electron gun are focused using the condenser lens and are directed towards the specimen (Figure 13). When the incident electron beam interacts with the specimen, different signals are emitted which give information about the specimen. The signal in the form of secondary electrons gives information of the surface topography and helps in producing Secondary Electron (SE) SEM images, the back scattered electrons give information of the density of minerals in the specimen, the diffracted back scattered electrons are used to determine crystal structure and orientation of minerals in the specimen and the characteristic X-rays provides elemental analysis of the specimen.
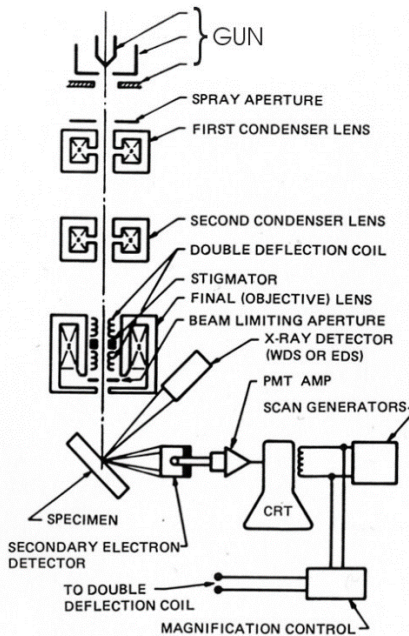
Figure 13. Schematic drawing of the electron and x-ray optics of a
combined SEM-EPMA (Swapp, 2017)

SEM provides a two-dimensional image of the specimen. Sample preparation for SEM imaging is crucial. SEM samples can be in powder form, bulk form or in liquid form. For bulk samples, the sample dimensions are approximately less than one inch. When the sample is imaged, only a small area of the whole sample is taken into consideration. Hence, multiple images from different regions of the sample is collected and analyzed. The size of the region imaged also depends on the resolution of the image required and the entities to be seen during the experiment. With a lower resolution, we will be able to image a large area of the specimen but we will not be able to identify the micro size entities in the specimen.

Chapter 3: Compressive Strength (UCS) tests on cylindrical shale specimens

The objective of this research was to investigate the effect of size on the strength of the shale specimens. To get an estimate of the strength of the sample, uniaxial compressive strength test was conducted. Ten specimens of size of 1.0, 2.0 and 3.0 inches were collected from the Marcellus shale outcrop in the New York region (Figure 14). Seven specimens were used for uniaxial strength test (UCS) and the remaining three were used for microscopic tests.
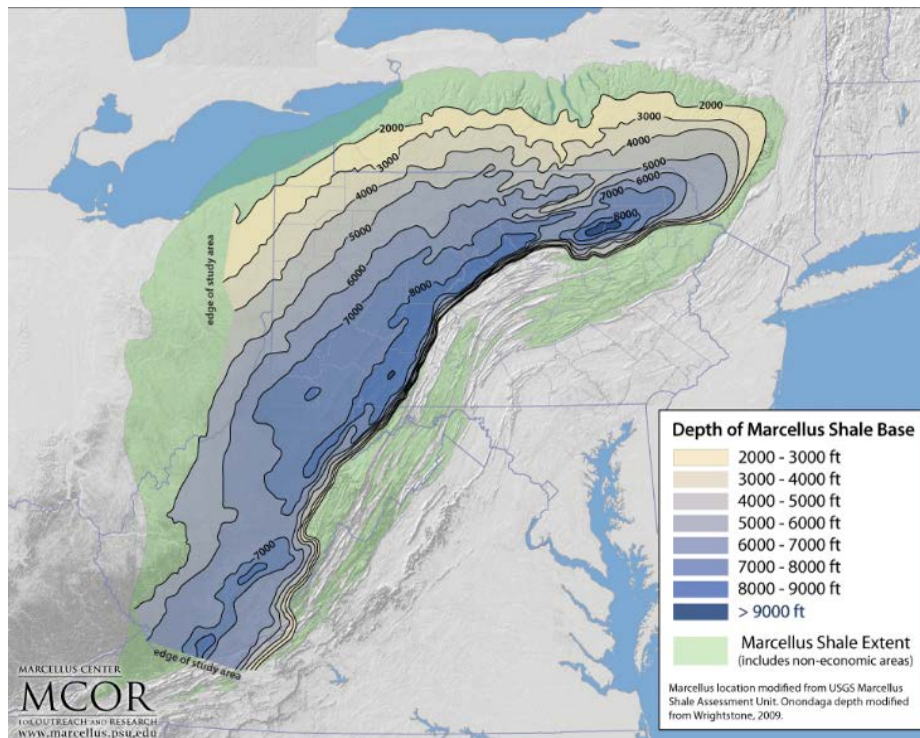
Figure 14. Marcellus shale formation extent (courtesy: MCOR)

3.1. UCS Test Setup:

Uniaxial compressive test was performed on the 3 different sample sizes in the rock mechanics lab at WVU. The sample sizes tested were 1", 2" and 3". Length over diameter ratio was maintained 2.0 for all the specimens. A constant loading rate of 100 psi/sec. was applied on the specimen during the test. Specimen were not exclusively prepared as cylindrical specimens that met the ISRM and ASTM standards were provided by the vendor. However, the specimens were checked

for any preexisting cracks and also the ends of the specimen to be parallel. The test was performed in a servo-control test rig. Figure 15 illustrates the servo-hydraulic Material Test System (MTS 440) used to perform the UCS test.

Figure 15. MTS servo-controlled compression testing system and its components- (1) Load frame (2) Hydraulic actuator (3) Strain gauge control panel (4) MTS data acquisition system (5) Computer (6) Upper steel platen (7) Lower steel platen

All the UCS tests were performed using the ASTM D7012 test procedures. The uniaxial compressive strength (σ_u) of the test specimen was calculated as follows:

$$\sigma_u = P/A \hspace{3cm} \text{Equation 8}$$

Where:

σ_u is the uniaxial compressive strength (UCS) in psi.

P is the failure load (lbs.) and

A is the cross-sectional area of the specimen (sq. in.)

Figure 16. Shale samples 1", 2" and 3" diameter used for UCS test

3.2. Test result:

The test results showed that axial splitting was the predominant failure mode (Figure 17). The specimens showed multiple failure cracks that developed along the axial length of the specimen. Axial splitting also indicate that the specimen had high degree of brittleness. There was a sudden release of stress after the maximum stress point exceeded.

Figure 17. Axial splitting failure of shale observed post failure

Figure 18 shows the stress against the strain plot as is usually observed in these types of tests. Initially, due to closure of pre-existing cracks as a result of loading, a nonlinear curve is observed at the initiation of the test. This is followed by a linear increase in stress and strain indicating elastic

21

behavior. When peak load is reached, specimen fails abruptly with loud noise depicting the brittle behavior of the shale tested. Table 3 gives the UCS values of the samples tested for each size.
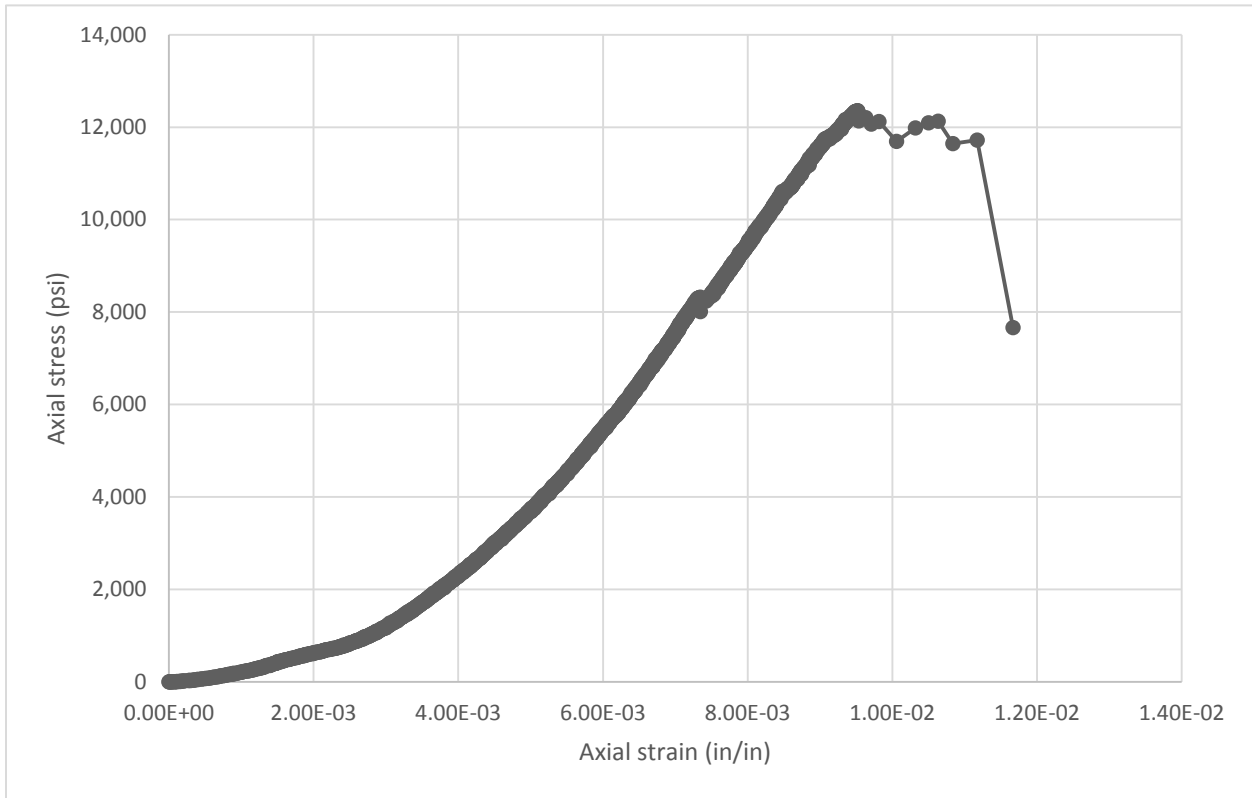
Figure 18. Stress-strain plot for shale specimen

Table 3. UCS (psi) of 7 shale specimens of 1", 2" and 3" diameter

Sl. No.	1.0 inch		2.0 inch		3.0 inch	
	Sample	UCS (psi)	Sample	UCS (psi)	Sample	UCS (psi)
1	MAR14	12,358	MAR24	11,185	MAR34	15,451
2	MAR15	16,267	MAR25	6,863	MAR35	11,469
3	MAR16	12,754	MAR26	6,738	MAR36	9,301
4	MAR17	11,515	MAR27	7,280	MAR37	11,102
5	MAR18	11,924	MAR28	7,005	MAR38	14,486
6	MAR19	13,134	MAR29	7,876	MAR39	12,570
7	MAR110	10,454	MAR210	7,507	MAR310	15,973

Box plot of the UCS test for the specimen shows that 2.0 inch specimens have the lowest strength compared to 1.0 inch and 3.0 inch specimens (Figure 19). The mean strength was similar

for 1.0 inch and 3.0 inch specimens. However, the spread of the strength values for 3-inch specimens was more than that of 1.0 inch specimens. The 2.0 inch specimen strength values had the least spread.

UCS for different size of specimen
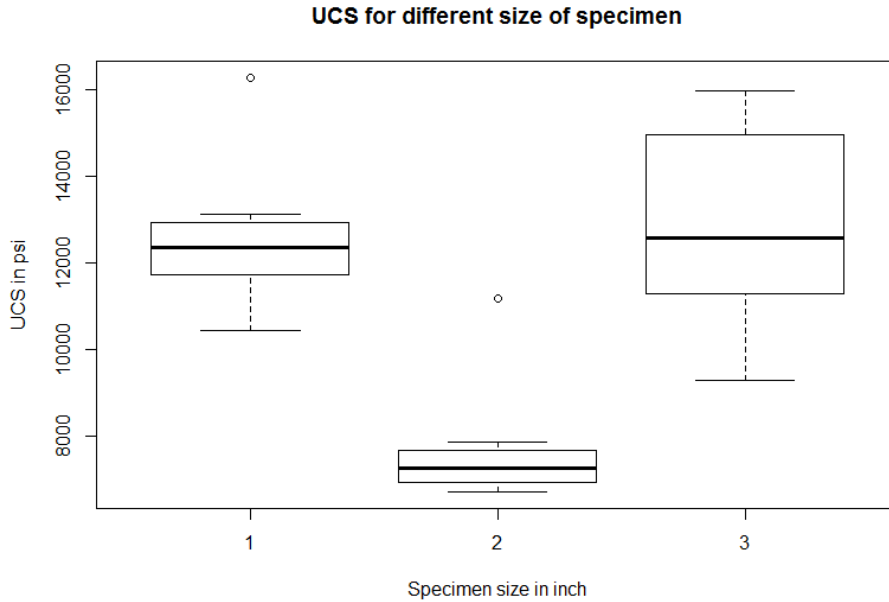
Figure 19. Box plot of UCS vs specimen size

The results are in contrast to the results observed in published literature. It has been seen from previous works by Bieniawski (1972) that below 2.0 inch diameter, the strength of the specimen is less. The strength peaks at 2 inch and then starts decreasing with a further increase in specimen size. For identifying the possible explanation for this variation in strength, characterization of the specimen is needed. From literature review (Chapter 2), it was found that grain size, grain shape, quartz content, grain orientation, porosity and micro-fractures influence the strength of rock. In current research, from preliminary investigation and vendor data, it was found that the porosity of the sample was between 2 to 4% and therefore, the influence of porosity was neglected. Also, from simple micro-CT scan, it was found that there was no significant inherent fracture network in the intact sample, so fracture parameters were also not included for the analysis. The other parameters and their effect on strength are discussed in Chapter 4 and Chapter 5.

3.3. Statistical analysis of strength of rock with size:

Statistical analysis was conducted with strength as a response variable and specimen size as a factor. Prior to the development of a statistical model, the data used in the analysis must satisfy the pre-existing conditions. The conditions to apply regression analysis and develop a one-way ANOVA (analysis of variance) model is described in the sections that follow:

Condition 1- Normality of residuals: Residual of a data value is defined as the absolute difference between the data value and the mean of the distribution. It checks whether the residuals obtained follows a normal distribution. This is performed by observing the normal quantile plot. In the normal quantile plot, if the residuals lie along the straight line passing through the center and do not fall outside the 5% significance level boundary shown in dotted line, then the data passes the normality of residuals condition. In the normal quantile plot shown in figure 20, most of the observations are along the straight line which satisfies the condition for normality of residuals.
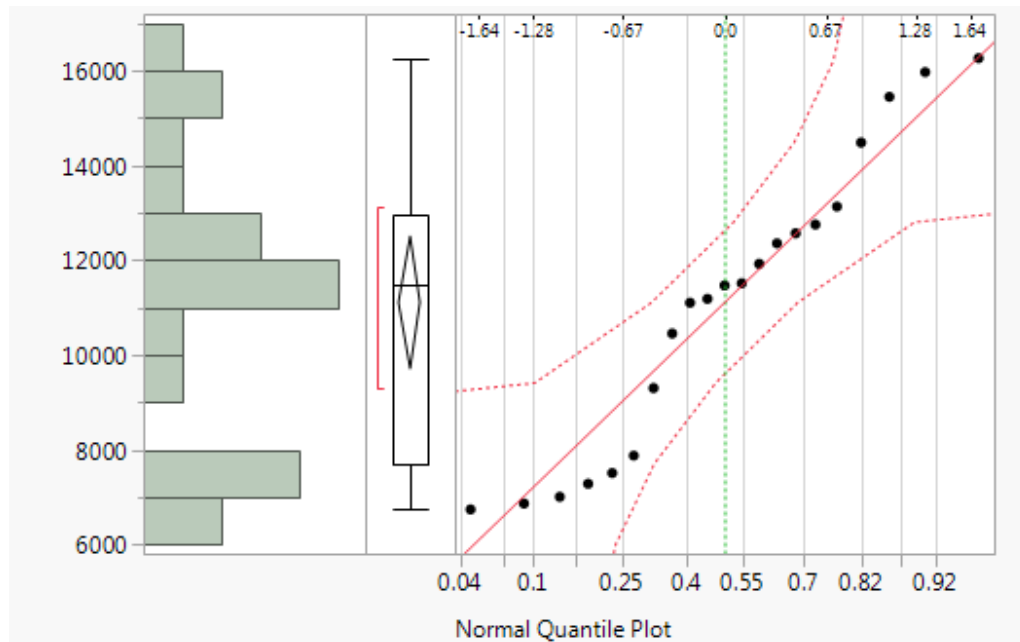
Figure 20. Normal quantile plot of the strength variable (plot obtained using JMP Pro13)

Condition 2-Constant variance condition: Constant variance condition checks if the spread of the residual strength calculated is almost similar or not. The spread is determined by calculating the standard deviation for the predicted strength of each factor level. In figure 21, three different colums of data set is observed in the plot. It was observed that the width of the three columns is

24

almost similar, which proved that the variance is almost same for the different levels of predicted strength.
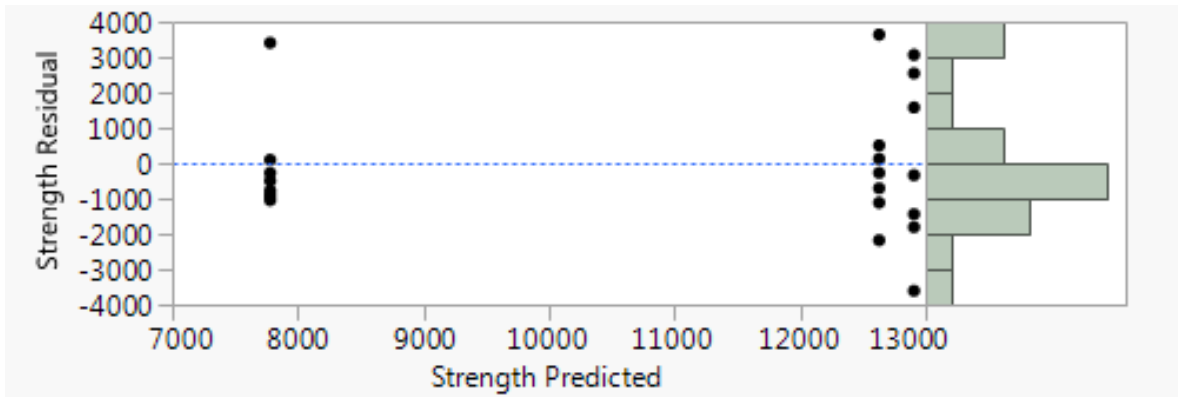
Figure 21. Residual vs predicted plot of strength variable to check constant variance condition (plot obtained using JMP Pro13)

Condition 3- Independence of residuals: The UCS tests were performed independent of each other. The UCS strength test performed on one sample was not related to test on another sample. Therefore, the strength data obtained was mutually independent which made the residuals independent of each other.

As all the three preconditions to perform the regression analysis and ANOVA model are satisfied, we move on to perform regression analysis.

3.3.1. Regression analysis:

Regression analysis establishes a relationship between the response or dependent variable (strength) and the factor or independent variable (specimen size). The relationship is given the form of an equation which best describes the trend in the data. To optimize and obtain the best possible representation of the trend, the error between the predicted variable (obtained from the equation) and the actual variable is minimized. That error is represented by the residual sum of squares (RSS) which is defined as:

$$RSS = \sum_{i=1}^{n}(y_i - f(x_i))^2 \hspace{3cm} \text{Equation 9}$$

Where RSS = residual sum of squares

y_i = response as obtained from the test for the ith variable

$f(x_i)$ = response as obtained from the equation representing the trend for the ith variable

n = number of samples

From Figure 22, a non-linear trend is observed for the response variable (strength). Different fits (linear, quadratic, cubic, and exponential) were tested to see which one fits the trend best (for which RSS is minimum). It was found that quadratic fit was the best.
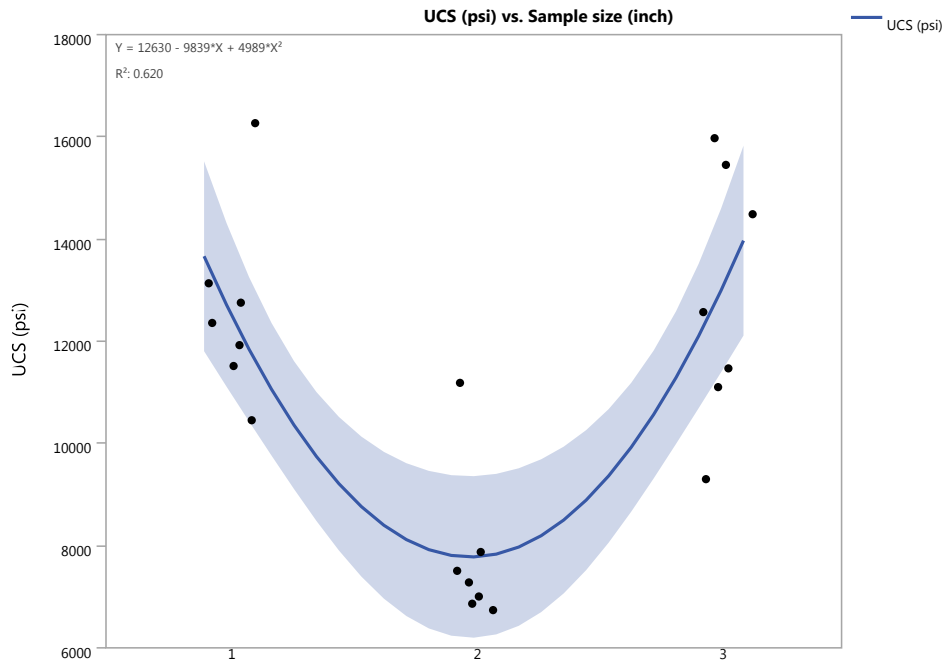
Figure 22. Regression plot for developing the relationship between strength and size (graph developed in JMP Pro13)

The equation best representing the trend can be written as:

$$Y = 12630 - 9839 \times X + 4989 \times X^2 \qquad \text{Equation 10}$$

Where Y = strength of the sample (in psi) X = sample size (in inches)

It is to be noted that this equation explains 62% of the variation observed in the data.

3.3.2. ANOVA model:

One-way analysis of variance is a technique to establish any significant difference between the means of two or more independent groups. The effort in the analysis is to find significant difference between the strength of different sized samples. The approach can be used for the whole model or for individual pairwise models.

26

3.3.2.1. Whole model analysis:

The strength as the dependent variable is referred here as a response variable and specimen size as an independent variable called as factor. Three different specimen sizes – 1, 2 and 3 inches are called levels. Therefore, one-way ANOVA analysis of the model was performed with strength as the response variable and specimen size as factor with 3 levels (1, 2 and 3 inch). From figure 23, it is observed that the p-value for the model is less than 0.05 showing that the model is significant at 5% significance level. Therefore, there is a significant difference in the mean strength between different sizes of the specimen.

Analysis of Variance

Source	DF	Sum of Squares	Mean Square	F Ratio
Model	2	116433289	58216644	14.6930
Error	18	71319437	3962191	Prob > F
C. Total	20	187752726		0.0002*

Figure 23. ANOVA model report for strength analysis (report obtained using JMP Pro13)

3.3.2.2. Pairwise comparison:

The pairwise comparison analysis compares the mean strength of a pair of specimen size and investigates any statistically significant difference between the mean strength of the two sizes. It is normally performed after the overall model is proved to be significant. Result of pairwise comparison is obtained in the form of an ordered differences report in JMP Pro13. From figure 24, the pair of 3.0 and 2.0 inch and 1.0 and 2.0 inch are significant at 5% significance level as the p-value for these pairwise comparison is less than 0.05. This shows that there is a significant difference in the mean strength between 3.0 inch and 2.0 inch samples and 1.0 inch and 2.0 inch samples. However, the difference in the mean strength between 3.0 inch and 1.0 inch sample is not significant at 5% level of significance.

Ordered Differences Report

Level	- Level	Difference	Std Err Dif	Lower CL	Upper CL	p-Value	
3	2	5128.140	1063.981	2892.80	7363.480	0.0001*	
1	2	4850.251	1063.981	2614.91	7085.592	0.0002*	
3	1	277.889	1063.981	-1957.45	2513.229	0.7969	
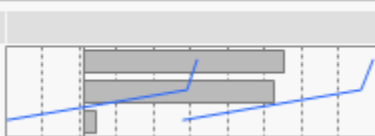
Figure 24. Ordered differences report for Sample size vs Strength paired comparison

Chapter 4: Composition analysis using X-ray Diffraction (XRD)

Srodon et al. (2001) observed that for identification and quantification of all minerals present in clay-rich rock, X-ray powder diffraction is needed. However, analysis of clay in a specimen remains a challenge even after availability of modern software and good mineral databases (Brindley, 1980). Therefore, sample preparation is of utmost importance when clay minerals are to be identified.

4.1. Sample Preparation for XRD

4.1.1. Crushing

The intact rock specimen was placed in a jaw crusher (figure 25). The mechanical pressure on the rock was developed by the two jaws of the crusher of which one was fixed while the other reciprocated. Minimal gap was left between the lower ends of the two jaws so that lowest size crushed particles could be obtained.

Figure 25. Jaw crusher (Mineral Processing Lab, WVU)

4.1.2. Grinding

The crushed specimen was then placed into a ball mill (figure 26) which works on the principle of impact and attrition. Size reduction is performed by impact as the balls drop from near the top of the shell. The crushed rock was ground for 20 minutes in the ball mill to reduce the particles to micron scale.

Figure 26. Ball mill (Mineral Processing Lab, WVU)

4.1.3. Sieving

The crushed particles obtained were now sieved with a No. 325 mesh (44 micron) sieve to get fine particles with size range below 44 microns. The main objective of reducing the size of the sample particles was to provide random orientation to the clay particles in the sample so that they can be quantified properly. In bulk form, they have a preferred orientation which makes their detection difficult. XRD analysis using bulk samples were also conducted and the results are discussed in Appendix A. The powdered samples collected were then used for XRD analysis.

4.2. Test setup for XRD analysis

XRD test was carried out using the PANalytical X'Pert Pro X-ray Diffractometer (Figure 27) of the WVU Shared Research Facilities. The analysis of the data obtained was done using Highscore software.

Figure 27. PANalytical X'Pert Pro X-ray Diffractometer (WVU SRF)

The powdered samples were put into discs as shown in Figure 28 and put in the sample slot in the diffractometer. The major points to be noted in the test were:

- Powdered samples were used
- Spinner sample stage was used
- Scan axis- Gonio
- Scan angle: 20˚ to 70˚ with step size of 0.01˚
- Scan type: Continuous
- Generator settings: 45mA, 45 kV
- Divergence slit type: Fixed
- Divergence slit size: 0.5˚

Figure 28. Powdered samples for XRD test

4.3. XRD Test result

From the diffraction pattern shown in Figure 29, it can be seen that almost all the major peaks have calcite in them. Montmorillonite is also widely distributed in the pattern. The major elements detected from the analysis are quartz, calcite, pyrite, fluorite, montmorillonite and apatite and illite in some samples.
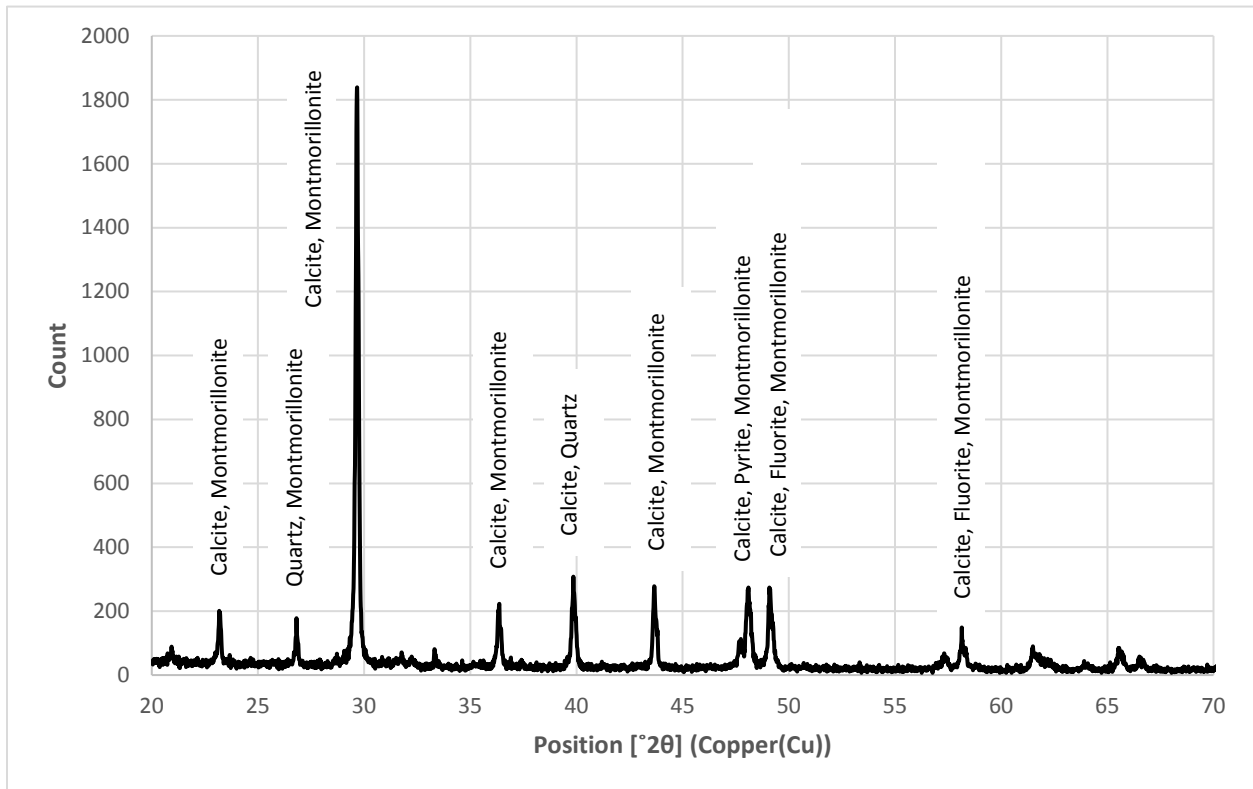
Figure 29. X-ray diffraction pattern for powdered shale sample

Quantitative distribution of the minerals in the powdered sample can be seen in the pie-chart shown in Figure 30. It is observed that calcite forms the bulk of the sample with close to 70%. Montmorillonite clay is also present at 18%. There is also presence of quartz, pyrite and fluorite at 4-5%. Table 4 gives information about the 10 powdered samples tested for each size and the quantitative composition of each powdered sample.
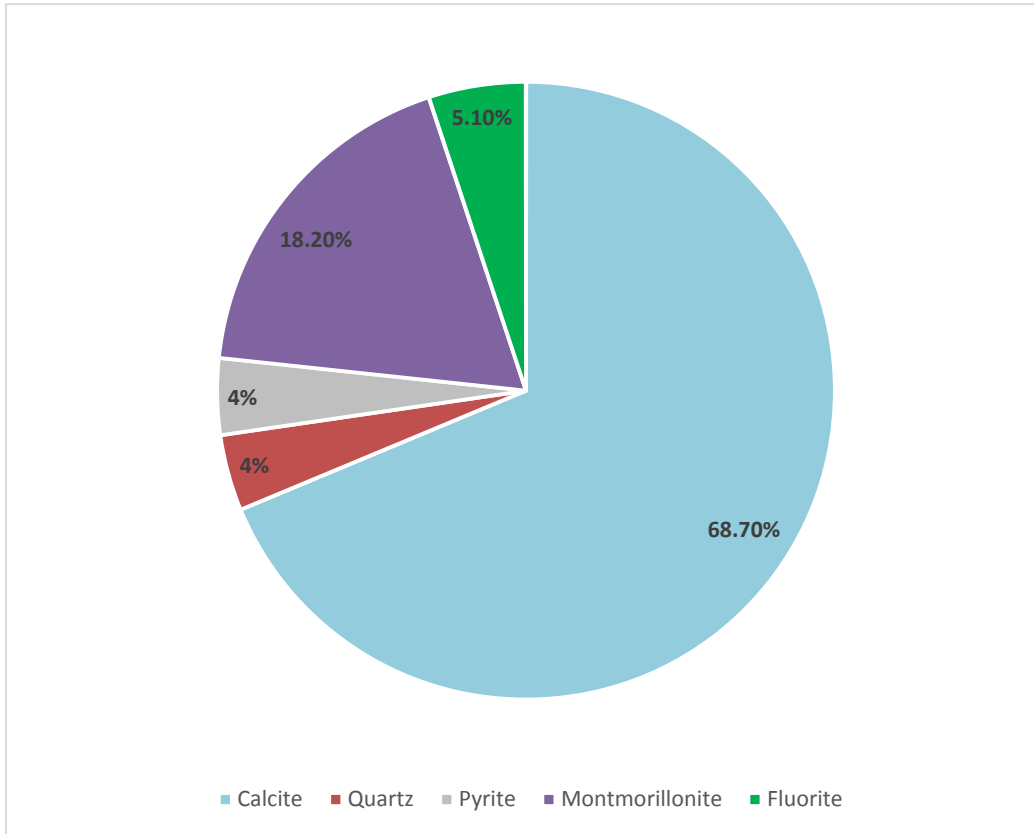
Figure 30. Simple quantitative estimation of minerals in XRD test

Table 4. XRD test result for 10 powdered shale samples each of 1 inch, 2inch and 3 inch size

ID	calcite	quartz	montmorillonite	ilite	fluorite	pyrite	apatite
1 inch sample							
P11	68.3	5.9	18.8		5.9		1
P12	56	8	17		4	6	9
P13	80	11			7		2
P14	90	8			2		
P15	80	14			6		
P16	63	7	25		5		
P17	84	10			6		
P18	84	10			6		
P19	78	12			10		
P110	82.2	9.9			7.9		
Avg.	**76.55**	**9.58**	**20.27**		**5.98**	**6**	
Error	**10.67**	**2.43**	**4.20**		**2.15**		**4.36**
2 inch sample							
P21	62	4	29		5		
P22	84	9			7		
P23	87	7			6		
P24	79.8	8.1			6.1	6.1	
P25	70	6	15			9	
P26	74.3	5.9			6.9	12.9	
P27	35	2	60		1	2	
P28	89	8				3	
P29	68.7	4	18.2		5.1	4	
P210	66	7	18		7	2	
Avg.	**71.58**	**6.1**	**28.04**		**5.51**	**5.57**	
Error	**15.78**	**2.19**	**18.64**		**1.99**	**4.09**	
3 inch sample							
P31	66	8		21	5		
P32	82	11			7		
P33	83.2	9.9			6.9		
P34	69	7	16		8		
P35	87.1	10.9			2		
P36	75.2	9.9			6.9	7.9	
P37	63	5	26		6		
P38	84.8	7.1			8.1		
P39	73.3	8.9			6.9	10.9	
P310	84	8			8		
Avg.	**76.76**	**8.57**	**21**		**6.48**	**9.4**	
Error	**8.65**	**1.91**	**7.07**		**1.84**	**2.12**	

4.4. XRD Test result analysis:

Ten samples in each size range were analyzed for their mineral composition. For getting the samples, the tested rock cores in each size range were crushed, ground and sieved. Then, the fine powder obtained was used to generate 10 different slices which were mounted on the XRD sample holder as shown in Figure 28. The mineral composition of the 10 samples in each size range is shown in Table 4 and their averaged values are shown below in Table 5.

Table 5. Average values of quartz, calcite, fluorite and clay in different sized shale samples

Specimen Size (inch)	Strength (psi)	Quartz (%)	Error Quartz (%)	Calcite (%)	Error Calcite (%)	Fluorite (%)	Error Fluorite (%)	Clay (%)	Error Clay (%)
1	12629	9.58	2.43	76.55	10.67	5.98	2.15	20.27	4.20
2	7779	6.1	2.19	71.58	15.78	5.51	1.99	28.04	18.64
3	12907	8.57	1.91	76.76	8.65	6.48	1.84	21	7.07

Figure 31 provides a visual representation of the composition analysis with respect to strength and size. It is observed the average strength of 1.0 inch and 3.0 inch specimen is same whereas the strength of 2.0 inch specimen is significantly lower. This is discussed in Chapter 3.
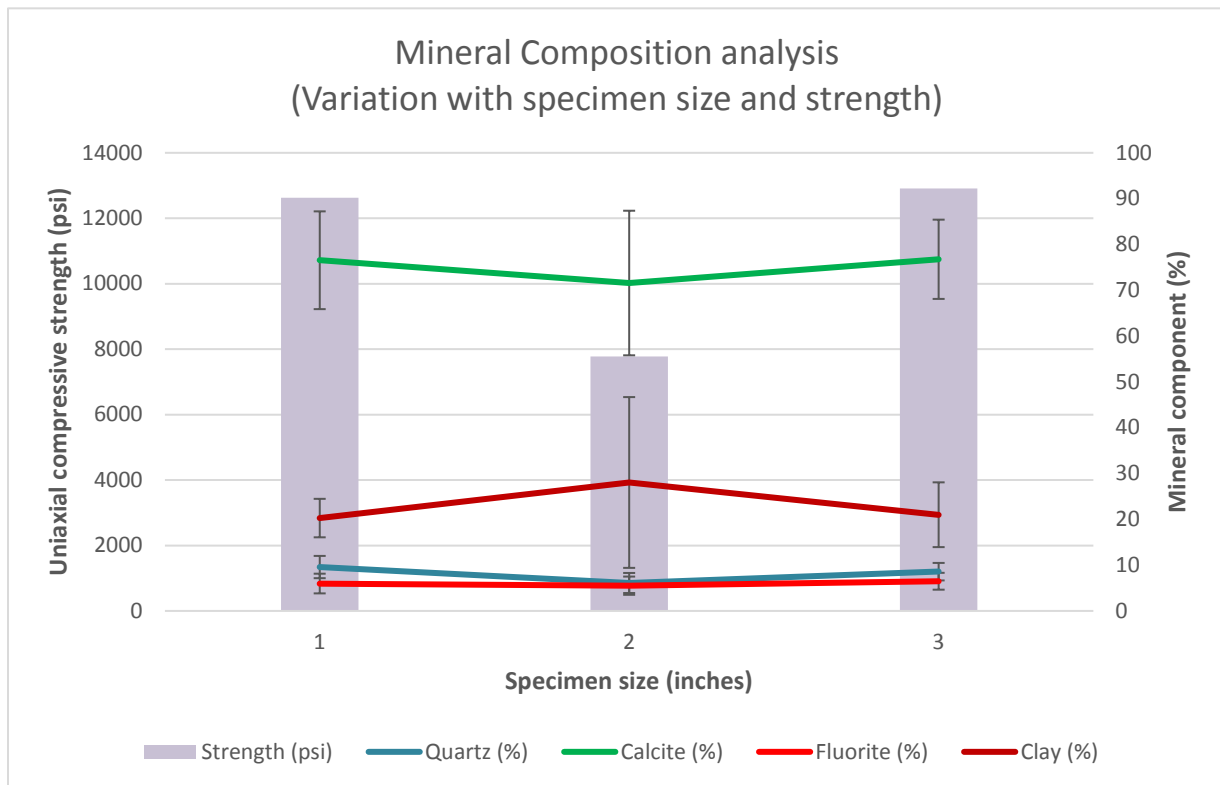
Figure 31. Correlation between strength of shale sample and its composition

Quartz, calcite, fluorite and clay content, which affects the strength of the shale sample are discussed in the sections that follow.

4.4.1. Quartz content analysis

Quartz content is lower for 2.0 inch specimen as compared to 1.0 inch and 3.0 inch specimens. The difference in quartz content of 1.0 inch and 3.0 inch specimens is not significant. This corroborates studies by Smart, Rowlands and Isaac (1982), Shakoor and Bonelli (1991) and Gunsalles and Kulhaway (1984) which state that increase in quartz content increases the strength of rock. Average quartz content is low in 2.0 inch specimen which contributes to its lower strength.

4.4.2. Calcite content analysis

Calcite (or carbonates) forms intermediate strong fraction in shales as evidenced by Rybacki, Reinicke and Meier (2015). Calcite forms the major component of the Marcellus shale tested as it forms almost three-fourths of the sample. Calcite also follows a similar trend as quartz with lower percentage of calcite in lower strength 2.0 inch specimens and comparatively higher percentage in 1.0 inch and 3.0 inch. As calcite forms an intermediate strong fraction in shale, higher percentage increases strength as is observed in the analysis.

4.4.3. Fluorite content analysis

Fluorite also follows a similar trend as the above two with lesser fluorite content in weaker 2.0 inch specimens and more fluorite content in stronger 1.0 inch and 3.0 inch specimens. However, as the percentage composition of fluorite is less (close to 6%) and as quartz has lower potential to influence the strength of the rock.

4.4.4. Clay content analysis

From Table 3, it is observed that clay was not found in many of the samples tested, however was quantified in the remaining samples. This showed that clay is present in the tested specimens however is unevenly distributed. In the samples in which clay was found, the average clay was around 20%. Figure 31 shows that the average clay content of 2.0 inch specimen is higher which strengthens the fact that clay contributes in reducing the strength of shale.

Chapter 5: Grain parameter analysis using Scanning Electron Microscopy (SEM)

Scanning Electron Microscopy was used to image the surface of shale and identify the grain parameters like grain size, grain shape, grain orientation and grain angularity. There were several steps in the imaging process which are discussed in detail:

5.1. Sample preparation

5.1.1. Cutting

The rock cores to be tested were cut into smaller sizes (preferably 1.0" × 1.0" × 0.5") using a low speed saw shown in Figure 32. This prevented the development of fractures during cutting and the sample remained in an intact state.

Figure 32. Isomet Low speed saw for cutting shale rock

5.1.2. Polishing

Due to complex structural heterogeneity of shale rock, it is a challenge to perform petrographic analysis. The range of variation of grain size is large (in some cases from micrometer to millimeter) and the presence of matrix materials makes it difficult to delineate the grain boundaries. In addition, the surface is weak, therefore it gets easily damaged when polished. Several methods of polishing for varying amounts of time were attempted and have been discussed in detail in Appendix B. The

final method involved use of two 12″ diamond lapping films of 15 microns and 6 microns for 3 minutes and 2 minutes respectively. The films were firmly fixed on the disc of the polishing machine as shown in Figure 33. The disc then was then rotated at a speed of 250 rpm and the sample was manually held against the surface of the film to touch the film surface. Water was used as a lubricant to dissipate the heat produced. Following lubrication, diamond paste of 0.5 micron was put into a polishing cloth and the sample was polished for 2 minutes. Instead of water, green lube was used as a lubricating agent. Green lube is a medium viscosity hexylene glycol-based lubricant used for metallographic preparation. After each polishing step, the samples polished were placed in a beaker containing deionized water and then it was placed in an ultrasonic bath. It is important to note that when polished for a longer time, the finished surface gets distorted.
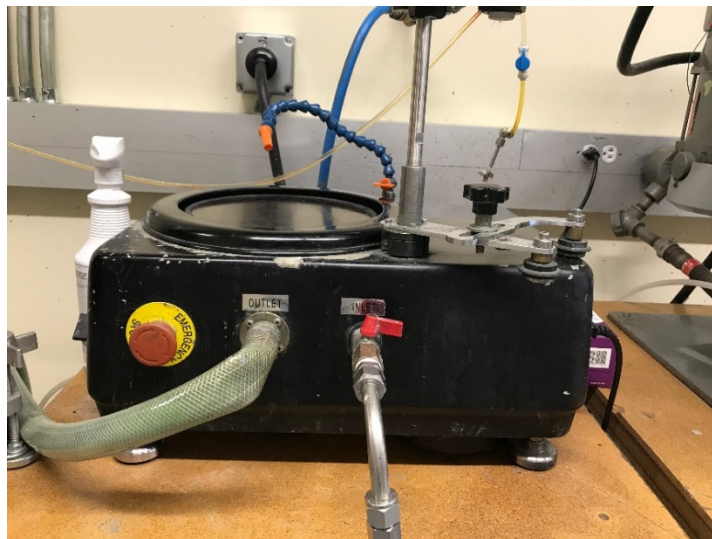
Figure 33. Sample polishing machine for polishing the shale sample

5.1.3. Etching

Etching was necessary to delineate the grain boundaries. As the sample contained a dominant percentage of calcite (from XRD analysis), etching was even more helpful. Different acids with different concentrations were used (Appendix B) to find the optimum solution which showed the maximum amount of grain boundaries. Maximum number of grain boundaries was observed when the polished shale sample was exposed to 0.2 M Hydro Chloric Acid (HCL) for one minute. The sample was then washed with deionized water and placed in an oven at 70˚C for 5 minutes. The length of exposure time is critical as HCL dissolves the calcite and matrix helps in visualizing the grain boundaries. However, when etching was used for more than 1 minute, there was a large

37

deposition of chloride on the boundaries that distorts the visualization. In addition, acid affects the soft shale by destroying the surface. A sample image of etching with 0.2 M HCL for 1 min is shown below:
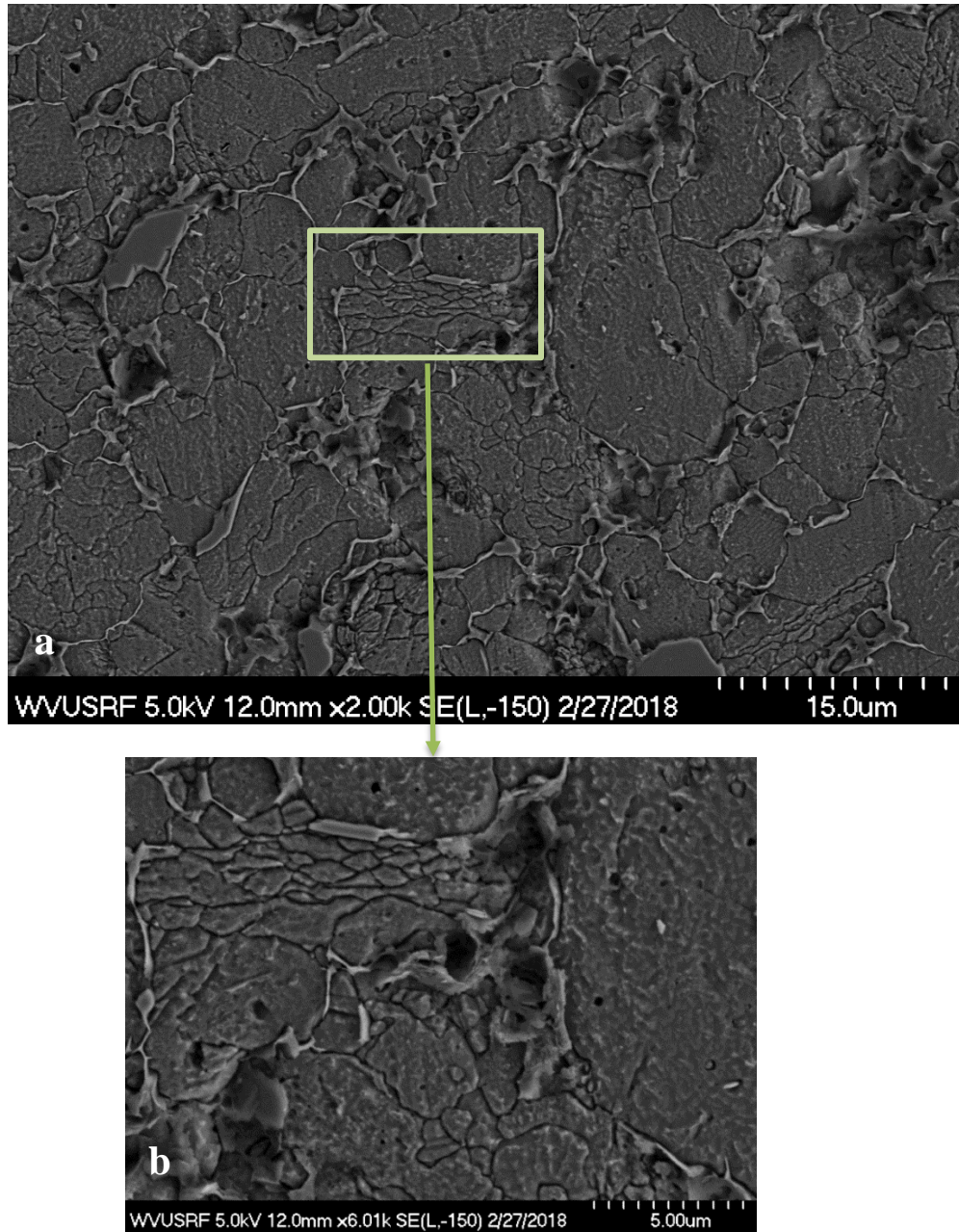
Figure 34. a. BSE image of polished shale sample etched with 0.2M HCl b. Magnified view of a small area to show the grains

5.1.4. Coating

The etched sample was then coated with Au using the Denton Desk Sputter as shown in Figure 35. As shale is composed of organic content it has the potential to absorb the incident electron when imaged in SEM. This degrades the quality of the image. Coating the specimen prevents electron from getting accumulated on the surface of the shale specimen.

Figure 35. Denton Desk V Sputter and Carbon Coater (WVU SRF)

The sample preparation steps for SEM imaging is summarized in the flowsheet as shown below.

Sample cutting (1"×1"×0.5") using low speed saw	→	Polishing using 15 micron DLF for 3 min	→	Ultrasonic bath for 5 min
Polishing using 0.5 micron DLF for 2 min	←	Ultrasonic bath for 10 min	←	Polishing using 6 micron DLF for 2 min
Ultrasonic bath for 10 min	→	Etching using 0.2 M HCl for 1 min	→	Washing the sample with deionized water
		Coating the etched sample with Au	←	Putting the sample in oven at 70˚C for 5 min

Figure 36. Flowsheet summarizing the sample preparation process for SEM imaging

39

5.2. SEM Imaging

Hitachi S-4700 Scanning Electron Microscope was used for imaging the surface of the shale samples. Both SE (Secondary electron) and BSE (Back scattered electron) multiscale imaging was performed on the shale specimens. A BSE image is depicted in Figure 37 and the different observations made are noted. We can see that there has not been siginifcant variation in the contrast of individual grains as most of the grains are calcite as the sample itself has about 70% calcite. Grains with higher density are lighter and pores are dark. A pyrite framboid is also observed in the image. It has a higher density as compared to other grains therefore it is lighter in contrast. There are few pores in the sample relative to the area imaged. The grains have a high range of variation and most of them are in the micron scale. Grains are relatively circular in shape and have random orientation.
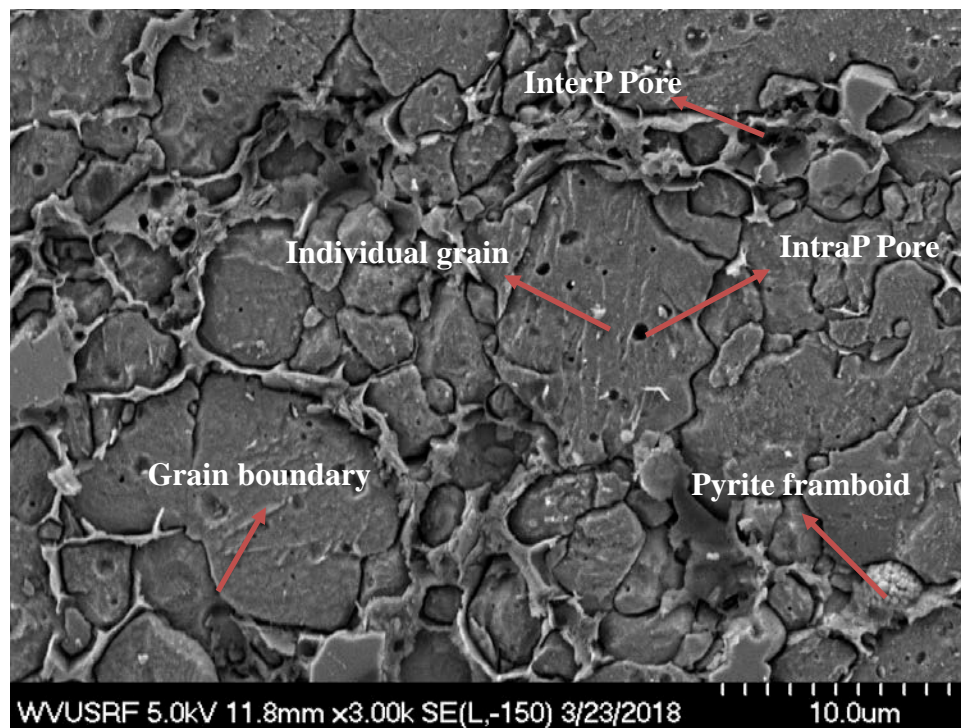
Figure 37. BSE SEM image of shale sample

5.3. Image Processing Technique

The grain boundary in the image obtained from SEM was digitized in Autocad® and the grains were completely darkened (Figure 38b) for easier thresholding. The automation

of this process was difficult as the sample is fairly homogeneous and there is no significant difference in contrast between different grains. If the sample is heterogeneous and contains different minerals, classification technique in ImageJ2 can be used and grains can be segregated mineral wise and individual information for each grain can be obtained as proposed by Krinsley, Pye and Tovey (1998).
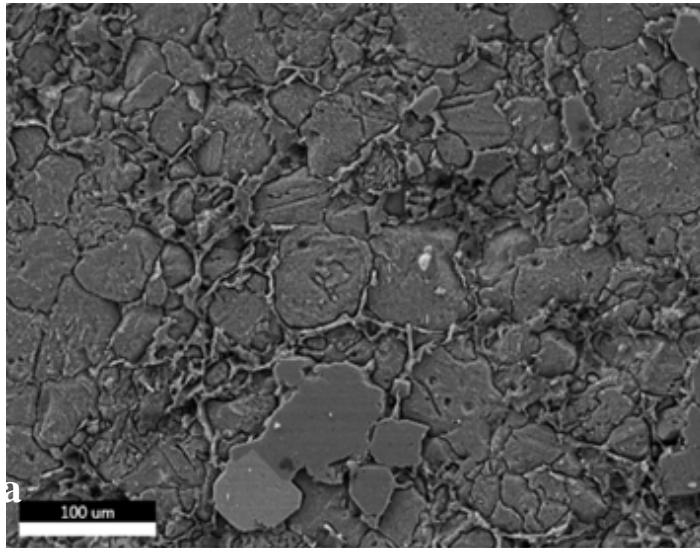
(a)
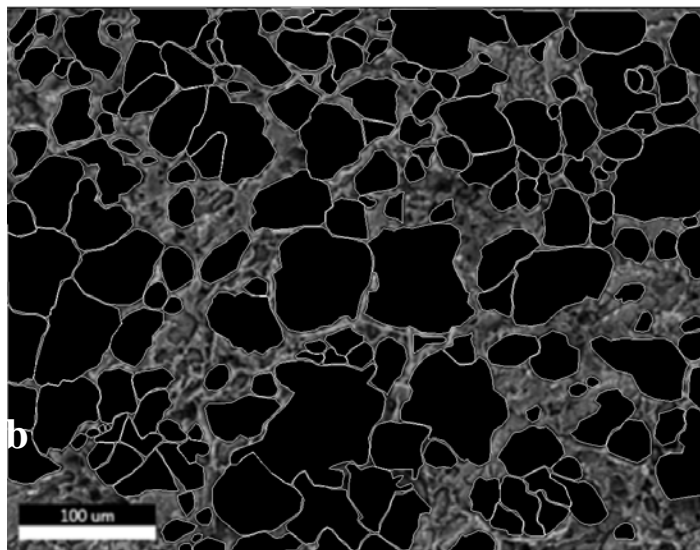
(b)

Figure 38. SEM image of shale a. Before digitization using AutoCAD b. After digitization using AutoCAD

41

The following steps were followed in ImageJ2 for analysis:

- Scale setting
- Checking the measurement scale
- Converting image to greyscale (8 bit)
- Thresholding the image
- Removing the scale bar
- Noise removal- remove outliers
- Separating the grain boundaries-
    - Binary - Erode
    - Minimum filter
- Analyzing the particles – selecting the parameters for measurement
- Measurement

Two major steps were thresholding and grain boundary separation which are discussed in detail:

5.3.1. Thresholding

Thresholding is a technique for dividing an image into two (or more) classes of pixels, which are typically called "foreground" and "background. A grayscale image is divided into two classes- black (pixel intensity 0) and white (pixel intensity 255). Figure 39a shows an SEM image which was digitized in Autocad®. The intensity histogram shown in the small box at the left top corner gives the distribution of the intensities of the different grains present in the grayscale image. The intensity histogram is a curve with two black vertical lines at 0 and 255 which indicates that there are grains with intensity other than 0 and 255. However, when the thresholded image in Figure 39b is analyzed, that the curve is not visible. Only two vertical black lines are visible at 0 and 255 positions. This showed that there are only two intensities in the thresholded image 0 and 255.
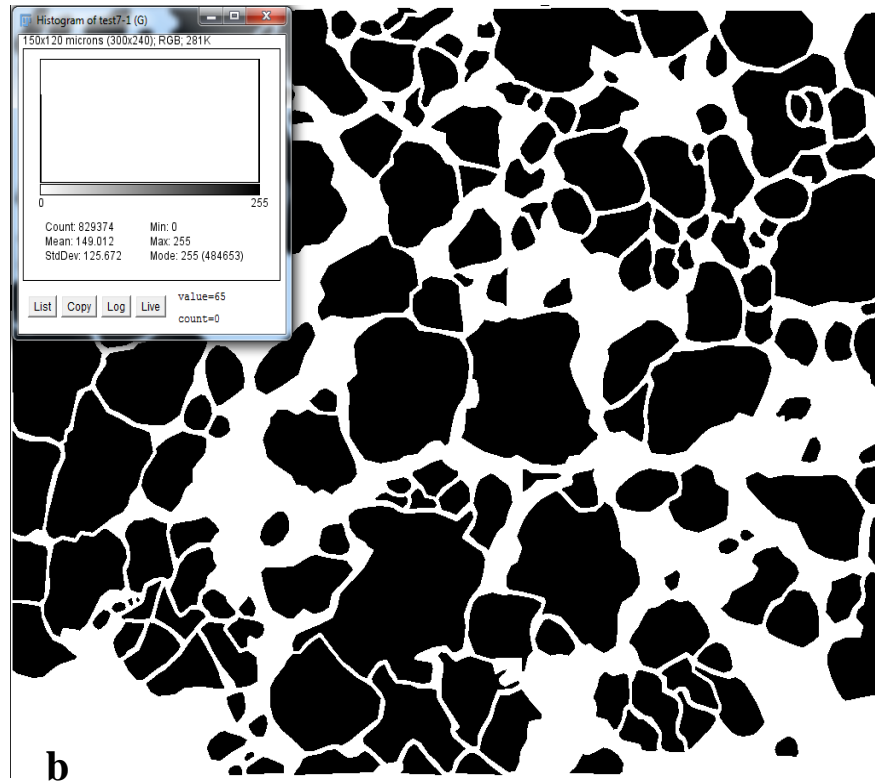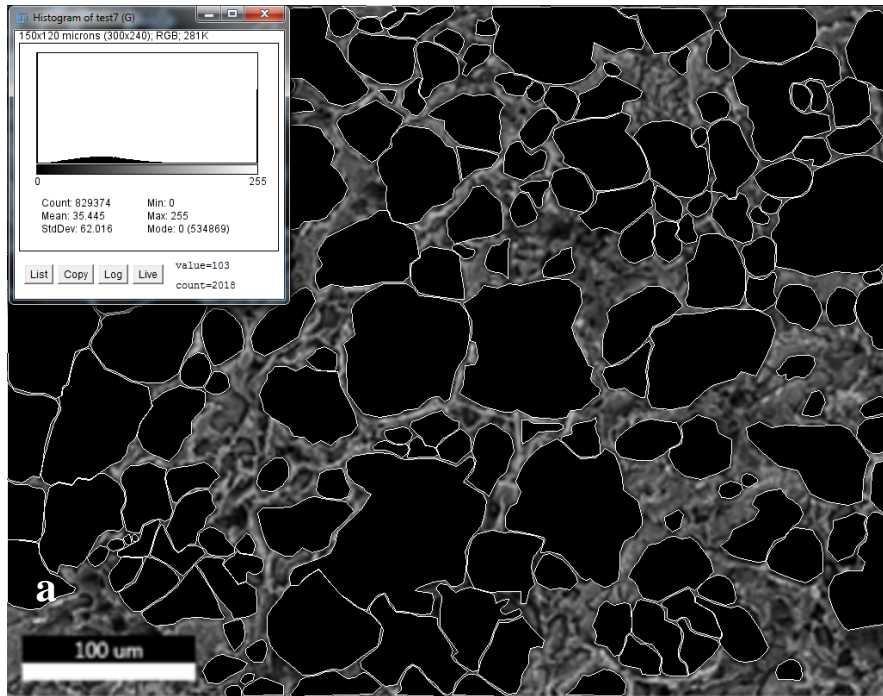
Figure 39. SEM images of shale a. before thresholding b. after thresholding

5.3.2. Grain boundary separation

One issue during petrographic analysis was grain boundary separation. For this purpose, minimum /maximum filter in ImageJ2 was used. In some cases, the grain boundaries of two adjoining grains were too close to be differentiated by pixels. When thresholding was performed, the boundaries would merge together and form a combined grain. Minimum filter reduced the size of each grains by 0.5 pixel which then separated the grains. It should be noted here that the loss in grain size was kept at minimum while increasing the grain numbers as seen through naked eye. An illustration of min/max filter is depicted in Figure 39. In Figure 40a, 122 grains were counted whereas after application of the filter, 188 grains were counted in Figure 40b.
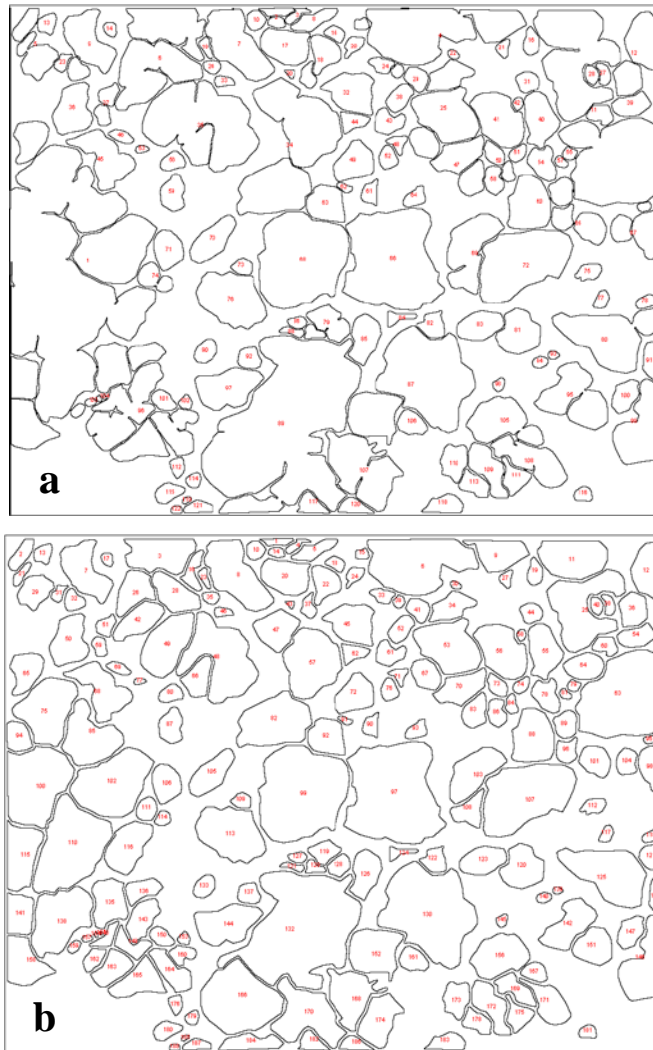
Figure 40. SEM image of shale a. before application of min/max filter b. after application of min/max filter

5.4. Grain parameters definition

Four grain parameters were analyzed- three of which were grain size, grain shape and grain orientation. The fourth parameter was texture coefficient which was derived from the former three.

5.4.1. Grain size

Grain size was measured using Feret's diameter. Feret's diameter represents the perpendicular distance between two parallel, outer tangents to an object. The longest diameter of an object is obtained by selecting the largest of the Feret's diameter measured in 32 different directions (e.g. at an angular resolution of 5.7˚). Minimum Feret's diameter is defined taking the shortest from 32 Feret diameters. The maximum and minimum diameters are not necessarily orthogonal as proposed by Ersoy and Waller (1995).
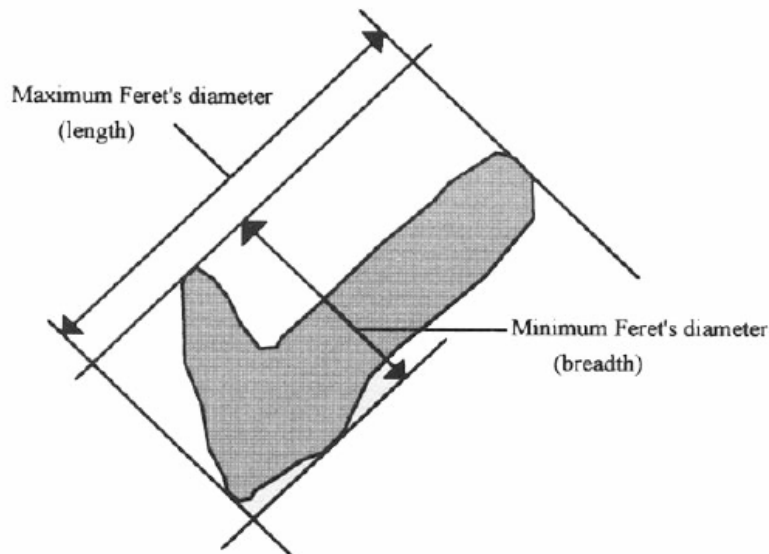
Figure 41. Maximum and minimum Feret's diameters (Ersoy & Waller, 1995)

5.4.2. Grain shape:

There are two secondary geometrical parameters in the analysis of grain shape: aspect ratio and form factor. Aspect ratio defines the elongation of the grains and is measured as the ratio of the grain's maximum and minimum Feret's diameter. Higher the aspect ratio more elongated is the grain. Form factor estimates the roughness of the grain's perimeter.

45

It is a measure of the grain's deviation from circularity. The circularity shape factor (form factor) of the grain is defined as:

$$Form\ factor\ =\ \frac{4\pi(area)}{(Perimeter)^2}$$
Equation 11

The value of form factor ranges from 0 to 1 with 0 for very rough objects and 1 for a perfect circle.

5.4.3. Grain orientation:

Grain orientation is estimated by a term called angle factor. For calculation of angle factor, a term called ANGLEDMAX, θ is calculated which is defined as the angle between the maximum Feret's diameter (length) and the horizontal direction. The maximum value of angle is 180˚. Angle factor is calculated only for grains whose aspect ratio (AR) is greater than two. The angle factor is calculated by a class weighted system applied to the absolute, acute angular differences (0˚<β<90˚) between each and every elongated grain according to Howarth and Rowlands (1987). Therefore, for a group of N grains the number of unique angular difference is:

$$(N-1) + (N-2) + \cdots + 2 + 1 = \frac{N(N-1)}{2}$$
Equation 12

The angular differences are grouped into nine classes, each of which are weighted.

Table 6. Classes and weightings for absolute, acute angular differences (Howarth and Rowlands, 1987)

Number	Class Range (β)	Weighting (i)
1	θ ≤ 10˚	1
2	10˚ < θ ≤ 20˚	2
3	20˚ < θ ≤ 30˚	3
4	30˚ < θ ≤ 40˚	4
5	40˚ < θ ≤ 50˚	5
6	50˚ < θ ≤ 60˚	6
7	60˚ < θ ≤ 70˚	7
8	70˚ < θ ≤ 80˚	8
9	80˚ < θ < 90˚	9

The angle factor is calculated by summing the class weighting and fractions of the total number of angular differences in each class.

$$\text{Angle factor } (AF_1) = \sum_{i=1}^{9} \left[\frac{X_i}{N(N-1)/2} \right] i \qquad \text{Equation 13}$$

Where, N = total number of elongated grains

X_i = number of angular differences in each class

i = weighting factor and class number

5.4.4. Texture coefficient

Texture coefficient is a combined parameter which takes into account the earlier three mentioned parameters as well as the degree of grain packing. Due to the difficulty in calculation of matrix content in the complex image obtained from SEM, the degree of grain packing was not considered. Therefore, a modified texture coefficient parameter was used as shown in Equation 14.

$$TC_m = \left[\left(\frac{N_0}{N_0 + N_1} \times \frac{1}{FF_0} \right) + \left(\frac{N_0}{N_0 + N_1} \times AR_1 \times AF_1 \right) \right] \qquad \text{Equation 14}$$

Where,

TC_m = Modified texture coefficient

N_0 = Number of grains with aspect ratio (maximum Feret's diameter or length to minimum Feret's diameter or breadth) less than 2.0

N_1 = Number of grains with aspect ratio greater than 2.0

FF_0 = Arithmetic mean of form factor of all N_0 grains

AR_1 = Arithmetic mean of aspect ratio of N_1 grains

AF_1 = Angle factor orientation which were computed for all N_1 grains

47

5.5. Grain parameters calculation and analysis

For estimation of all the parameters, approximately 500 grains of each size specimen (1″, 2″ and 3″) were selected, from which half were selected from the top sections and the other half from the cross-section. Varying number of images of each size was required to obtain 500 grains. Only those grains were considered for digitization which was delineated easily through unassisted vision. The grains were then digitized using AutoCAD® software and thresholded and processed using ImageJ2. Once the final image was obtained, the grain parameters were analyzed and reported.

5.5.1. Grain size analysis:

Grain size is represented by maximum Feret diameter. Maximum Feret diameter for each grain for each sized specimen was calculated and averaged to obtain an average grain size for each of 1″, 2″ and 3″ sample as shown in Table 7.

Table 7. Average grain size for each shale sample size along with their average strength

Sample size (in)	Strength (psi)	Avg. Grain size (micron)	Error Avg. grain size (micron)
1	12,629	7.43	4.35
2	7,779	11.99	8.37
3	12,907	7.66	3.80

From the plot in Figure 42, it is observed that 2.0 inch sample has a higher average grain size than 1.0 and 3.0 inches. In addition, figure 42 also shows that the average strength of the 2.0 inch specimen was the lowest than the other two specimen groups. No significant difference between the average grain size of 1.0 and 3.0 inch specimen was observed and their average strength also showed the similar trend. Therefore, it can be proposed that grain size affects the strength of the rock. Rocks which have larger grain size have less strength compared to rocks having smaller grain size.
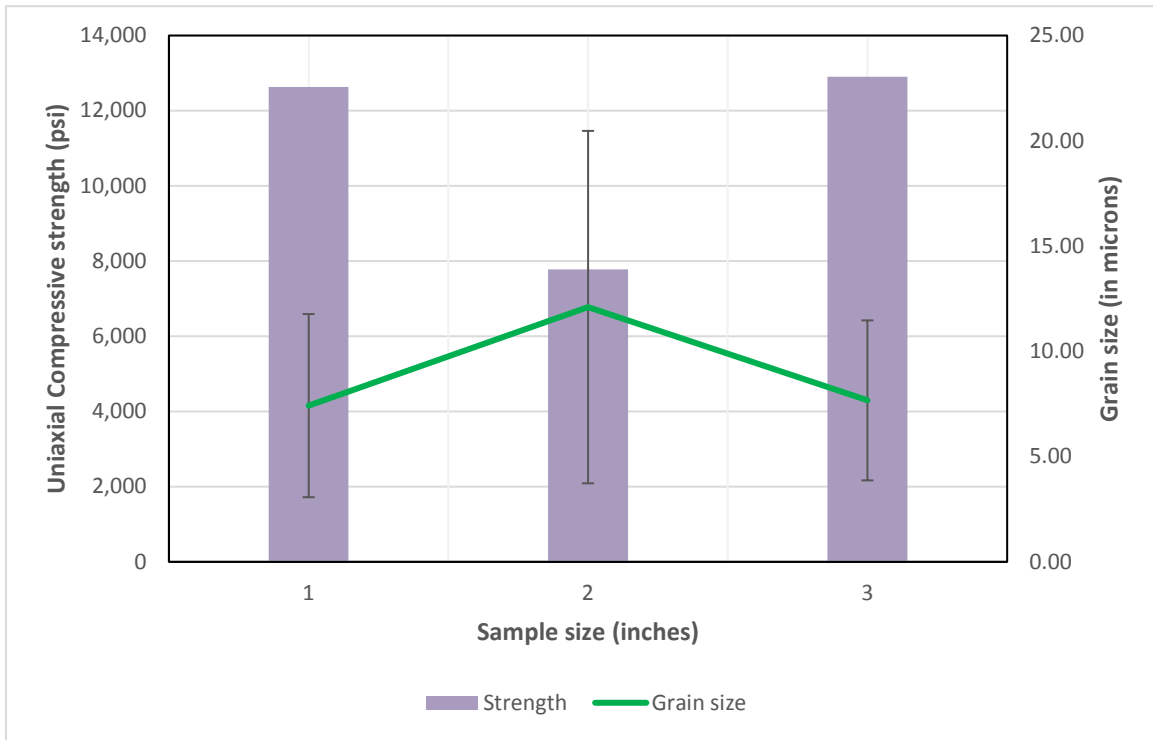
Figure 42. Relationship between shale rock strength and grain size

5.5.2. Grain shape analysis

Grain shape is represented by aspect ratio (AR) and form factor (FF). Aspect ratio defines the elongation of the grains and form factor denotes the roughness of the grain boundary. As reported earlier circular grains have low compressive strength and grains with rough surface have higher compressive strength. Aspect ratio was calculated by dividing the maximum Feret's diameter with minimum Feret diameter. Form factor is calculated using perimeter and area of the individual grains. The average values of AR and FF are tabulated below in Table 8.

Table 8. Average AR and FF for each shale sample size along with their average strength

Sample size (in)	Strength (psi)	Grain shape (AR)	Error (AR)	Grain shape (FF)	Error (FF)
1	12,629	1.57	0.85	0.69	0.10
2	7,779	1.52	0.38	0.68	0.10
3	12,907	1.57	0.45	0.72	0.09

From Figure 43, it is observed that the average AR is low for 2.0 inch specimen and maximum for 3.0 inch specimen. Again, the difference in AR of 1.0 and 3.0 inch specimen is very low. This is in agreement with literature by Fahy and Guccione (1979) that proved that grains with low aspect ratio have lower strength. The results are validated from earlier reported literatures as circular grains are not tightly packed and can disintegrate easily under stress, whereas elongated grains pack more tightly and therefore are difficult to break under stress.

In this analysis, form factor is not in agreement with earlier findings reported in various literature. Less value of form factor portrays a rough surface which increases the strength of the specimen, however in this analysis, 2.0 inch specimen has the lowest form factor whereas 1 inch and 3 inch have higher form factor. In addition, the difference between the form factor values is less and is nearly same for all the specimen sizes. Therefore, it is concluded that form factor cannot be considered as an important parameter to quantify strength.
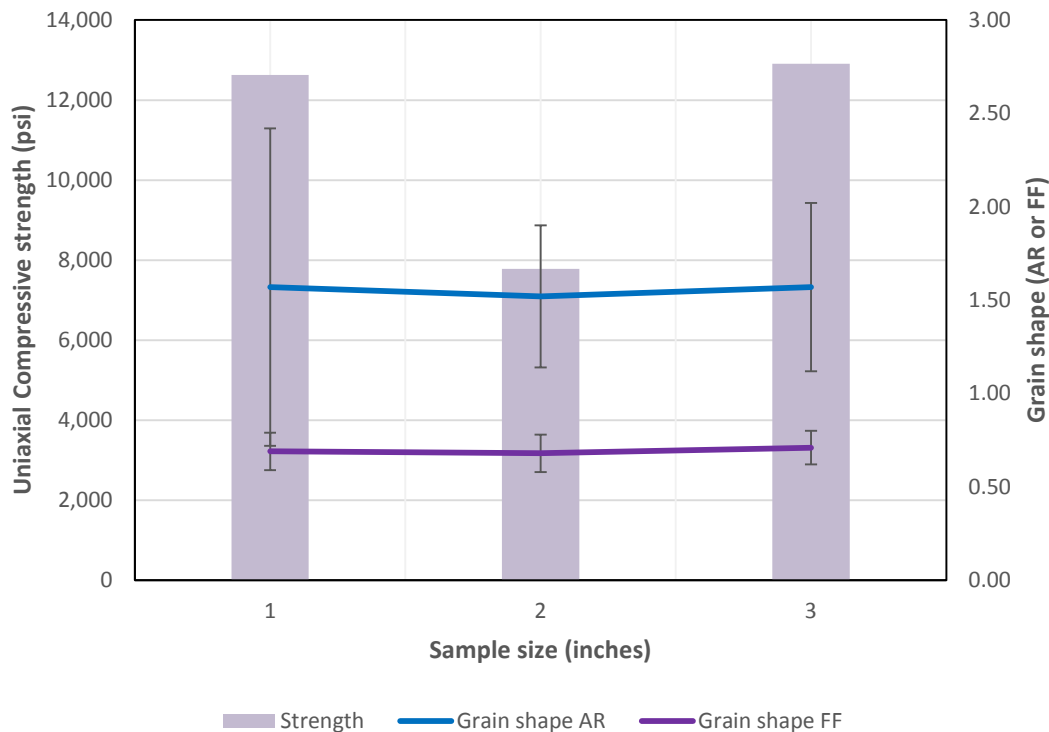
Figure 43. Relationship between shale rock strength and grain shape

5.5.3. Grain orientation analysis

In Figure 44, an illustrative SEM image is shown to explain the calculation of angle factor which represents grain orientation. There are 52 grains delineated in the SEM image. Out of them, angle factor is calculated with only those grains whose aspect ratio is more than 2, i.e. elongated grains. Using the elongated grains, all possible combinations of the Feret angle is calculated and the angular difference of all the combinations are estimated. From all the calculated angular differences, only those differences are selected which are acute. The acute angular differences are then grouped into a table and weighted as shown in Table 9.
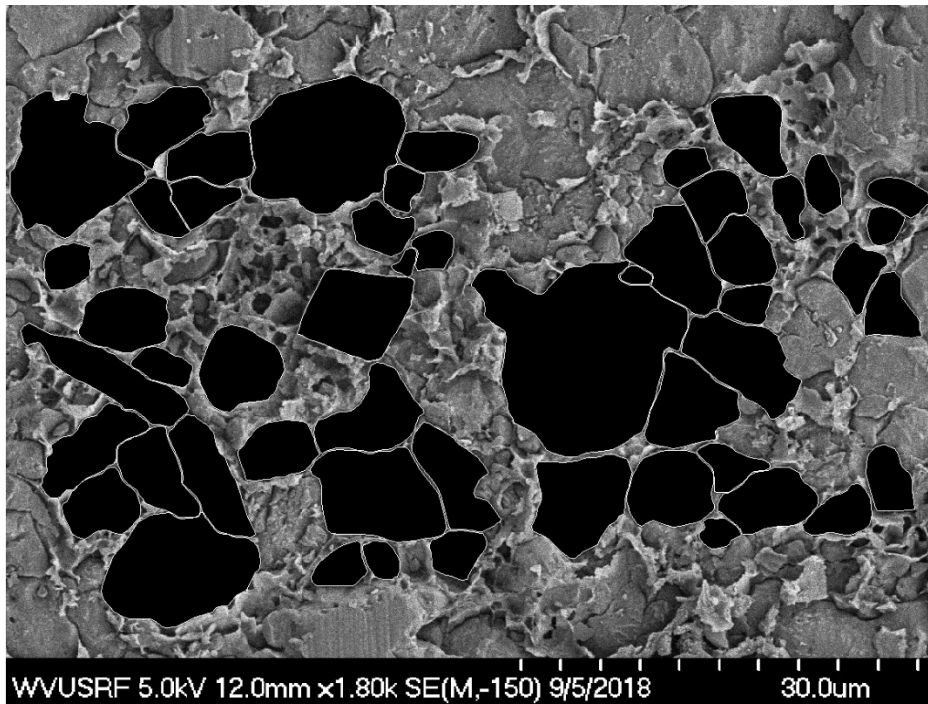
Figure 44. SEM image to illustrate grain angle factor calculation

Table 9. Weighting of acute angular differences to calculate angle factor for a shale sample

Class range	Number of angular differences (X_i)	Weighting (i)	$X_i * i$
$\theta \leq 10°$	1	1	1
$10° < \theta \leq 20°$	1	2	2
$20° < \theta \leq 30°$	4	3	12
$30° < \theta \leq 40°$	1	4	4
$40° < \theta \leq 50°$	2	5	10
$50° < \theta \leq 60°$	1	6	6
$60° < \theta \leq 70°$	1	7	7
$70° < \theta \leq 80°$	1	8	8
$80° < \theta < 90°$	3	9	27
Total	**15**		**77**

The angle factor is then calculated by summing the class weighting and fractions of the total number of angular differences in each class.

$$Angle\ factor\ (AF_1) = \sum_{i=1}^{9} \left[\frac{X_i}{N(N-1)/2} \right] i \qquad \text{Equation 15}$$

Where,

N = total number of elongated grains

X_i = number of angular differences in each class

i = weighting factor and class number

In this case, angle factor (AF_1) is 3.67. The angle factor is then divided by 5 to make the angle factor numerically similar to other parameters used to calculate texture coefficient as proposed by Howarth and Rowlands (1986). Modified texture coefficient is then calculated using Equation 14. Howarth and Rowlands (1987) and Ersoy and Waller (1995) reported that a higher angle factor denotes grains being more randomly orientated in a plane that produces higher rock strength. Rocks in which grains are less randomly oriented (low angle factor) tend to have lower strength. Modified texture coefficient is formulated as such that it is higher for rocks with higher strength. In the shale sample tested by us, most of the grains are circular (aspect ratio less than 2). From Table 10, less than 15% of the grains are

elongated in all the specimens and only elongated grains are used to calculate angle factor. Therefore, the grain orientation does not form an important parameter in this analysis for quantifying the strength. However, the plot showing the relationship between grain orientation and strength is shown in Figure 45.

Table 10. Average AF_1 and TC_m for each shale sample size along with their average strength

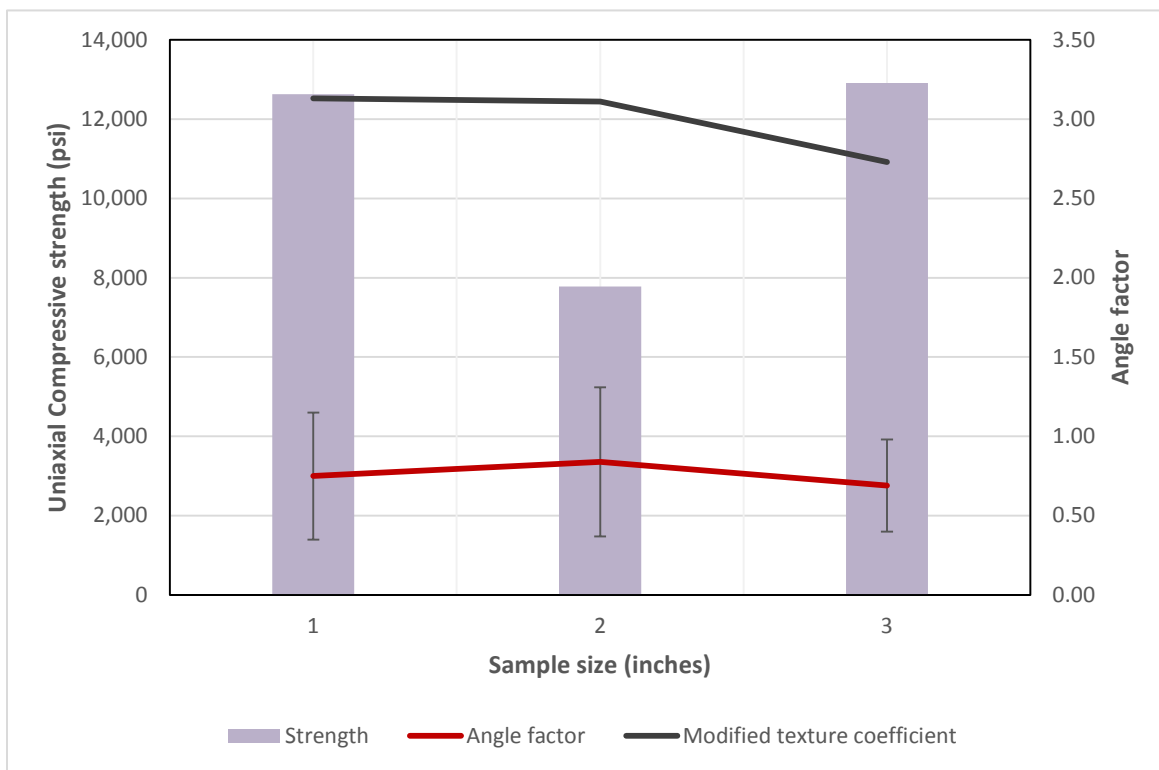| Sample size (in.)	Strength (psi)	Angle factor (AF_1)	Error in Angle factor	Modified Texture Coefficient (TC_m)	% of Elongated Grains
1	12629	0.75	0.40	2.94	10.1
2	7779	0.84	0.47	3.14	9.56
3	12907	0.69	0.29	2.57	12.37

Figure 45. Relationship between shale rock strength and grain angle factor and texture coefficient

53

5.6. Energy-dispersive X-ray Spectroscopy (EDS) Analysis

EDS provides an elemental information of the surface of the specimen. The information obtained can be then used for chemical characterization. In EDS, a high energy beam of charged particles or X-ray is focused on the specimen. When the ground state electrons of the specimen interact with the high energy beam, they are ejected from the shell and another electron from a higher energy level moves in to take the position of the ejected electron. In this process, the difference in energy between the two levels is emitted in the form of an X-ray. As this difference in energy is characteristic of the atomic structure of the element, the emitted X-ray carries information about the element from where it gets emitted.

In this analysis, EDS of an SEM image analyzed the distribution and quantification of the elements present in the image. The quantity of the element in any region helped in the identification of the compound or mineral present which further helped in the identification of the mineral grains in the SEM image. Figure 46 depicts the identification of each individual element in the sample. The percentage of each element in the area of analysis is also presented. Figure 46a shows the region of the sample used for EDS analysis. The resolution of the image is 5 microns. Figure 46b depicts an overlay of all the elements present in the region. Figure 46c shows the distribution of carbon in the region of analysis. It was observed that carbon is thoroughly distributed in the entire region and the concentration of carbon particles is not high. Figure 46d shows the distribution of oxygen particles in the analyzed region. It is observed that oxygen is also distributed evenly in the entire region however, the concentration is higher than that of carbon. The quantification table in the side shows that there is 20% carbon and 58% oxygen in the analyzed region. Figure 46e shows the distribution of silicon in the analyzed region. Silicon is concentrated in the center of the region. As oxygen is also present in the region, it is possible that the grain might be a quartz grain. Figure 46f shows the distribution of gold particles in the region analyzed. Au present in the sample is mainly due to the presence of Au coating which was done to prevent deposition of charge on the sample surface. From EDS, information is obtained on the distribution of different elements in the specimen. From the quantification of the elements present, we can analyze the mineral grains present. EDS is useful when only a small portion of the sample is analyzed. For example, in this analysis,

only 20×20 micron area was analyzed which also is one of the limitations of EDS. In addition, EDS is a time-consuming process. The accuracy of the results depends upon the duration of EDS. Therefore, EDS is not useful when the area of investigation is large.
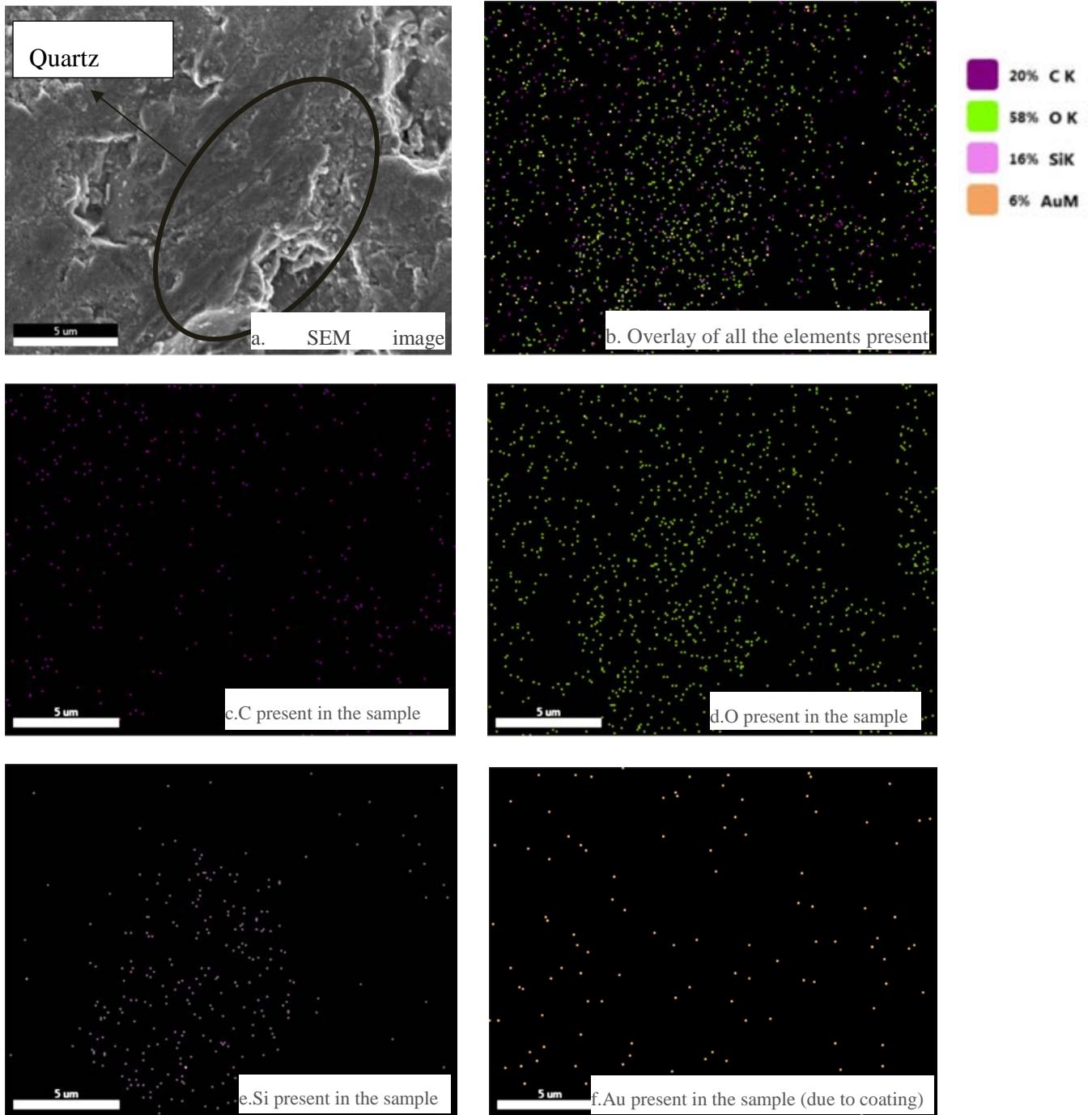

Figure 46.a-f. EDS analysis of shale sample

Chapter 6: Results and Conclusion

The aim of this study was to characterize shale rock using Scanning Electron Microscopy and X-ray Diffraction. The petrographic parameters investigated were then correlated with strength and size of the specimen. The results obtained are summarized below.

6.1. Summary of result:

- Size of the specimen was an important factor contributing to the variation in strength of the shale specimens.
- Quartz content influences the strength of shale rock. Strength of the rock decreases with low quartz content. 2.0 inch specimen which had the lowest strength had minimum quartz content.
- Calcite being a major component in composition analysis affected the strength of shale rock. Higher calcite content resulted in higher strength.
- Fluorite followed a similar trend as calcite with weaker samples having a lower average fluorite content.
- Clay was present in the shale sample studied. Clay being soft reduces the strength of rock. Clay was quantified being more in 2 inch samples than the other two sizes.
- For identifying clay, powdered samples should be used for X-ray diffraction analysis. Bulk XRD analysis was not able to identify the clay present.
- Shale has a complex microstructure so it needs to have a defined polishing methodology. Polishing should not be done for long as shale is also very soft.
- Etching forms an important part of sample preparation if petrographic analysis is to be done.
- The range of variation of grain size in the shale samples tested is very high, extending from a minimum of 0.16 micron to a maximum of 61.07 micron.
- Grain size is an important factor contributing to the strength of the shale samples tested. 2.0 inch specimens which had the lowest strength had a higher average grain

size compared to other specimen sizes. Therefore, higher grain size decreases the strength of the sample.

- Grain shape when defined by aspect ratio followed the general trend which showed that rocks with grains with higher aspect ratio has higher strength than the other rock types. However, no such trend was observed when form factor was used to define grain shape.

- There was no correlation between strength and grain orientation. Analysis showed that less than 15% of the grains were elongated which were used to quantify grain orientation.

6.2. Future research recommendation

- For size effect study, a very small range of the size effect curve has been analyzed. Bieniawski (1972) found that the strength of coal became constant after 65 inches. When similar analysis is performed for shale, then only 5% of the size effect range was analyzed in the current research. For a better understanding of size effect, the range of the specimen sizes tested should be increased.

- In addition to petrographic parameters, effect of fracture parameters and porosity should be investigated for shale.

- The specimens tested were very homogeneous with calcite being a major component. Therefore, the BSE images obtained from SEM did not have a distinct variation in contrast between different grains. Classification technique can be used to train the algorithm to quantify the petrographic parameters mineral wise.

- Grain orientation should be investigated using the EBSD (Electron Back Scattered Diffraction) detector of the SEM.

Appendix A

XRD bulk analysis

Before XRD powdered analysis was carried on, in order to get information on each of the samples tested, bulk analysis was performed. As, the samples retrieved post UCS test were really less (especially for 1 each), bulk form of each sample was used for XRD. Figure 47 shows some of the samples tested.

Figure 47. Bulk shale samples used for XRD analysis

Sample preparation

No specific arrangements for sample preparation was needed as there was no crushing or grinding involved. The sample bits obtained after UCS test were cut into appropriate shape (approx. 1.0 inch × 1.0 inch × 0.5inch) using low speed saw.

Test setup

All the settings used for powdered diffraction were used in this case also, except a change in the sample stage. Multipurpose sample stage was used instead of spinner type.

Test result

The diffraction pattern obtained from the test (Figure 48) is almost similar to that obtained in the powdered sample analysis. However, we were not able to identify the clay components present in the sample. In powdered diffraction analysis, we were able to detect clay in almost half of the samples tested. But in bulk analysis, there was no detection of clay. This elucidates the importance of crushing and grinding the sample. Clay, being amorphous, is difficult to detect when in bulk form. When finely grounded, preferred orientation of the clay particles is removed which makes their detection easier.
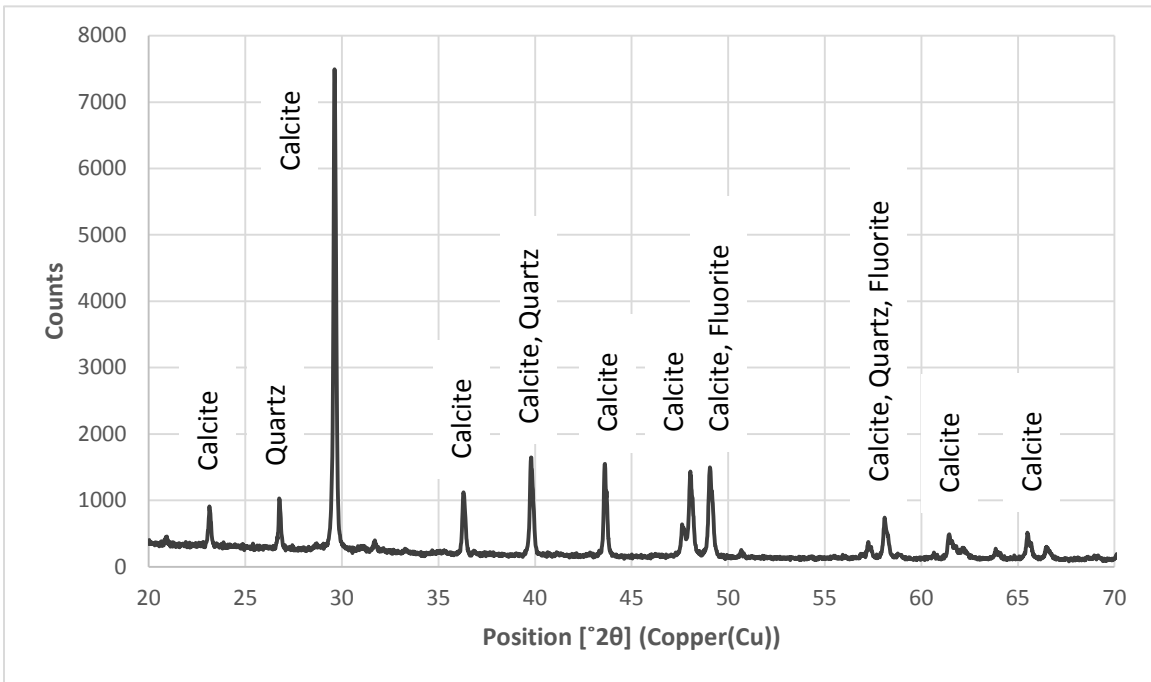
Figure 48. X-ray diffraction pattern for bulk shale samples

If we want to look at the result quantitatively, the major components were calcite, quartz and pyrite, with calcite ranging from 80-90% in most of the samples. This value got reduced to about 70% when powdered samples were analyzed. Quartz accounted for 2-10% and some of the samples had pyrite in the range of 5-10%. A quantitative pie-chart of one of the representative sample is shown in Figure 49.
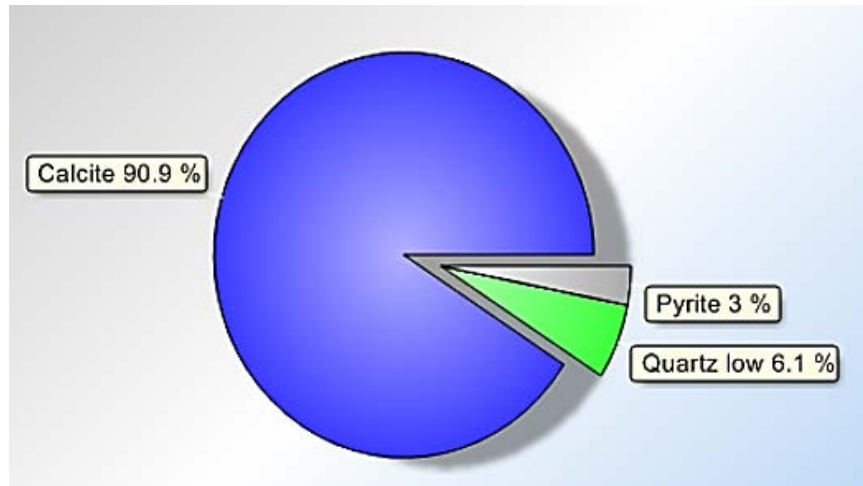
Figure 49. Quantitative pie-chart of bulk XRD analysis of a shale sample

Test analysis

Uniaxial compressive strength of the samples was plotted against calcite and quartz content in them as shown in Figure 50 and Figure 51 respectively. There was no significant correlation between the sample strength and its quartz and calcite content.

Figure 50. Correlation between UCS of shale and quartz content for bulk analysis using XRD

Figure 51. Correlation between UCS of shale and calcite content for bulk analysis using XRD

Appendix B

SEM Sample preparation iterations

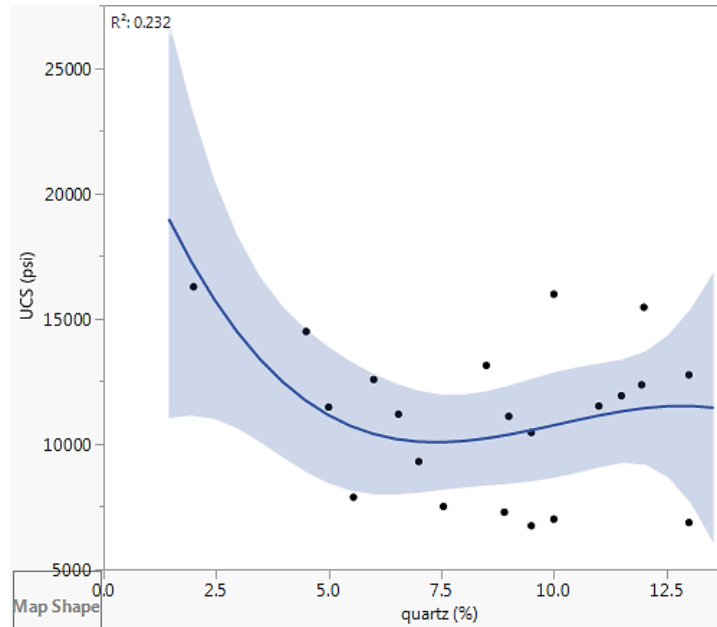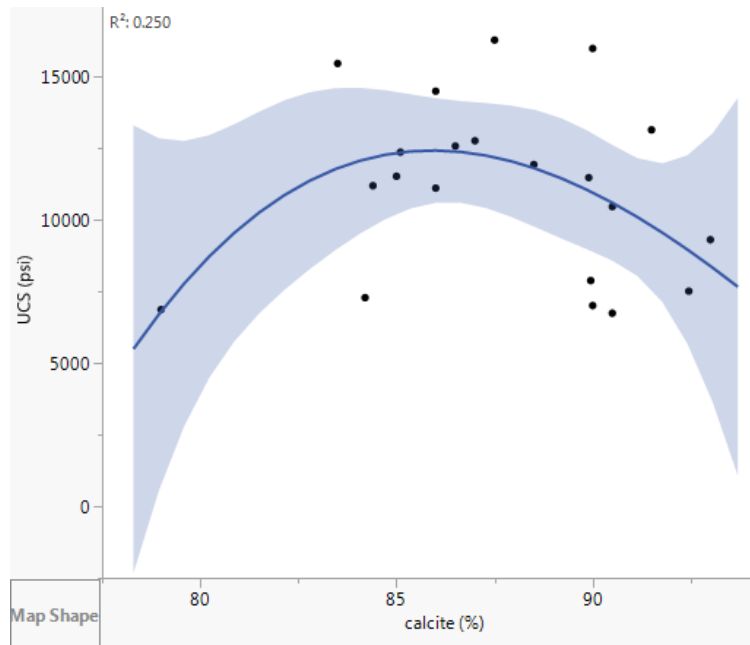Many iterations were performed by varying the polishing film thickness, polishing time, combining different set of polishing films and using different etching acids for variable times. These iterations were aimed at achieving the optimum image quality which can be used for further analysis. Some of these iterations and the images produced are discussed below:

Iteration 1

This was the base iteration. No polishing and etching was done. The sample was cut into appropriate size (approx. 1.0 inch $\times$ 1.0 inch $\times$ 0.5inch) and placed in the specimen chamber in SEM. The main purpose was to observe the quality of the image developed and the parameters to be improved. The SE image obtained is shown in Figure 52 which seems to be of very little use to us. Grains can't be delineated and the individual grains don't seem to be at the same vertical level.
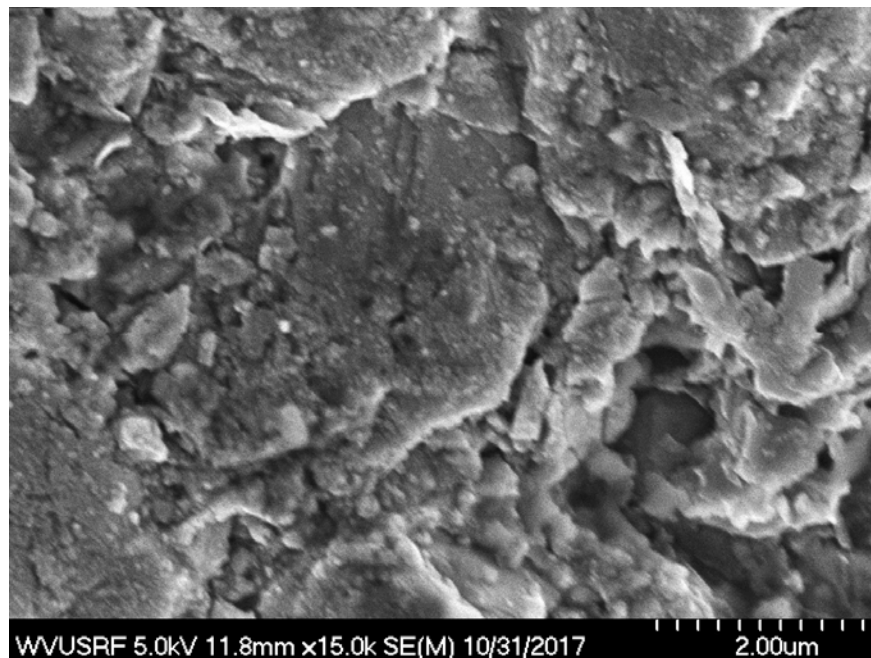

Figure 52. SEM image of shale without polishing and etching

Iteration 2:

The second iteration involved polishing the specimen with 500 grit SiC (35 micron) for 3 minutes and then with 30 microns, 15 microns, 6-micron diamond lapping film for 2 minutes. Then, for fine polishing, 0.5 micron diamond paste was used for 2 minutes. The specimen was then sputtered with Au to prevent deposition of incident electrons on the sample surface as the sample had organic materials. In the image obtained as shown in Figure 53, it can be seen that the surface has been destroyed (polished excessively) due to rough polishing by SiC. This tells us that the shale is really soft and SiC will not work for this type of sample.
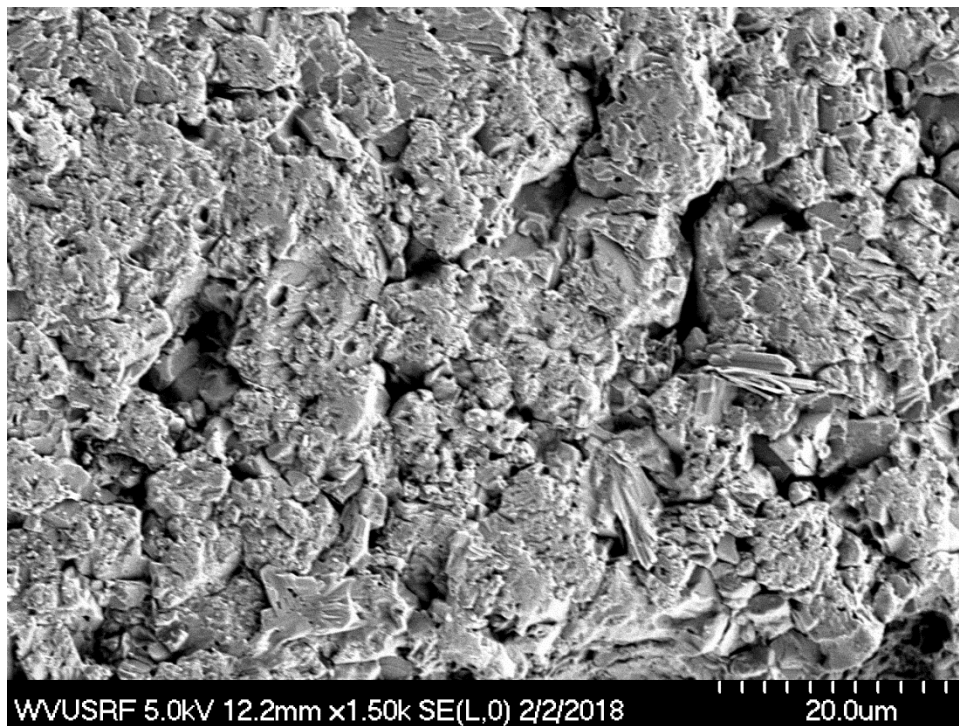
Figure 53. SEM image of shale with SiC, 30, 15, 6 and 0.5 micron polishing

Iteration 3:

In this iteration, the specimen is polished using a 30 micron diamond lapping film for 3 minutes and then with 15, 9 and 6 micron films for 2 minutes. Au sputtering was performed to prevent deposition of electrons on sample surface. In the image shown in Figure 54, a significant amount of authigenic minerals have developed on the surface. The image does not meet the required standards for grain parameter analysis.

63
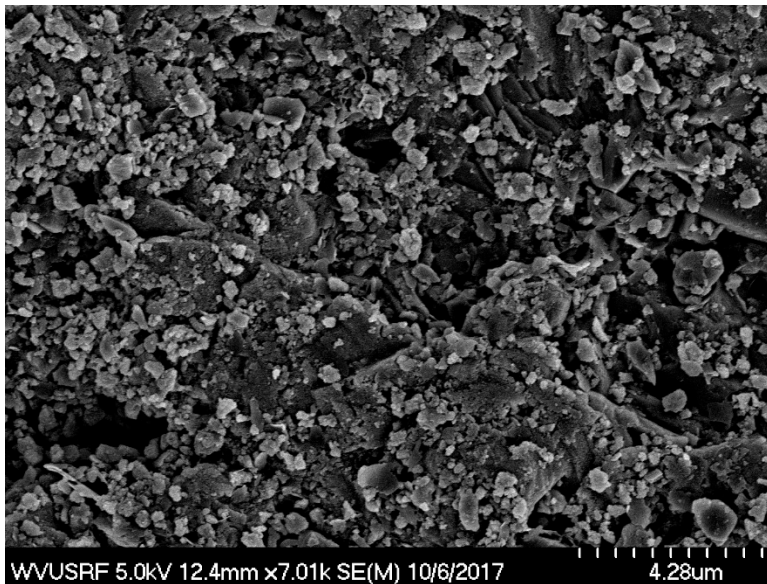
Figure 54. SEM image of shale with 30, 15, 9 and 6 micron polishing

Iteration 4:

From earlier analysis, 30 micron polish was not effective in polishing the specimen. Therefore, in this iteration, the specimen was polished with 15 micron film for 3 minutes and then with 6 and 0.5 micron films for 2 minutes each. Sample was then sputtered with Au. The image (Figure 55) meets the standards and the specimen surface is preserved. In addition, no authigenic minerals are seen on the surface. However, the individual grains are still not visible.

Figure 55. SEM image of shale with 15, 6 and 0.5 micron polishing

Iteration 5:

Etching was performed with 0.1M and 0.2M of HCL solution for 1 minute or 2 minutes. 0.1 M HCL solution for 1 minute gave a good result as shown in Figure 56. However, the grain boundaries are not distinctly visible. Therefore, 0.2 M HCL solution was used to etch and the results remarkably improved than the images obtained using 0.1 M HCL.
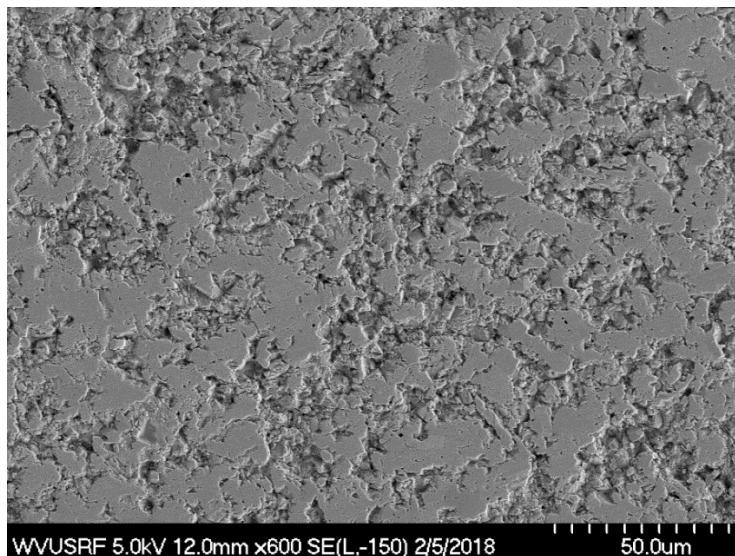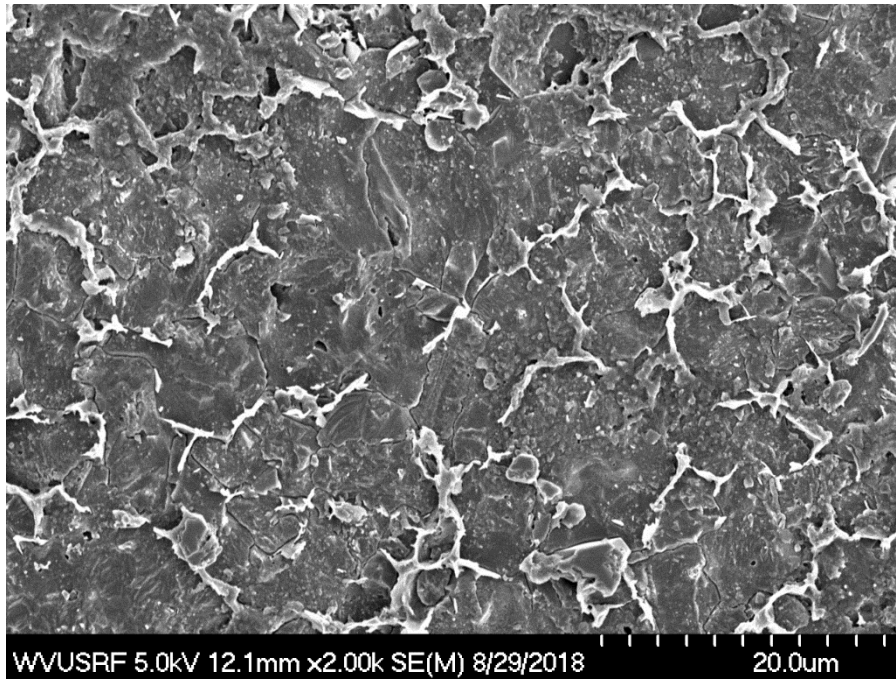

Figure 56. SEM image of shale etched with 0.1M HCl for 1 minute

It was also observed that when 0.2 M HCL was used for 1 or 2 minutes for etching, the images did not show any significant difference in the quality. Therefore, the images obtained from both durations were used for grain parameter analysis. In addition, as the objective was to visualize the grain boundaries, which are observed in both secondary electron (SE) images and back-scattered electron (BSE) images (Figures 57 and 58), both SE and BSE images obtained from this etching process were employed.
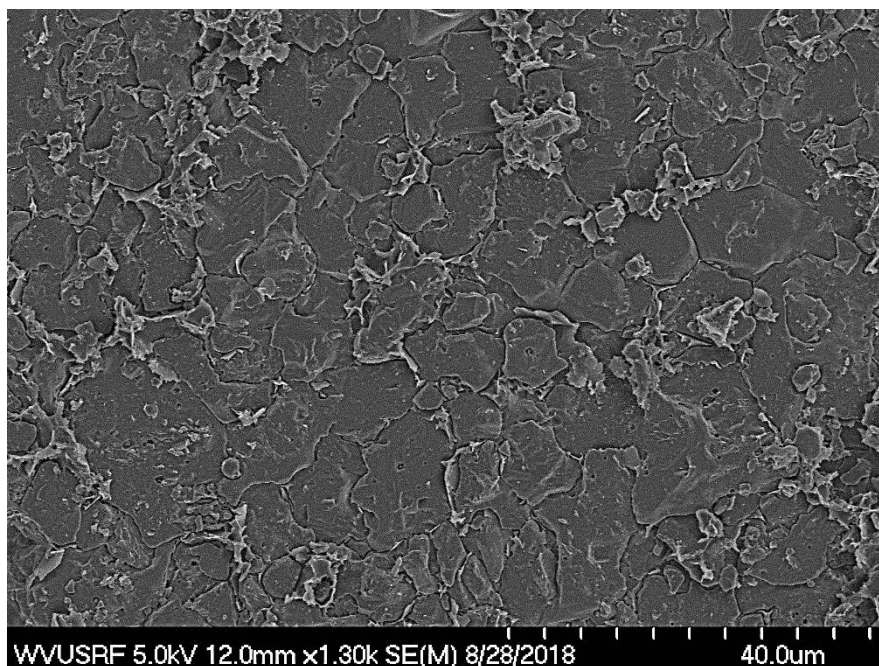
Figure 57. SE SEM image of shale using 0.2M HCl for 1 minute
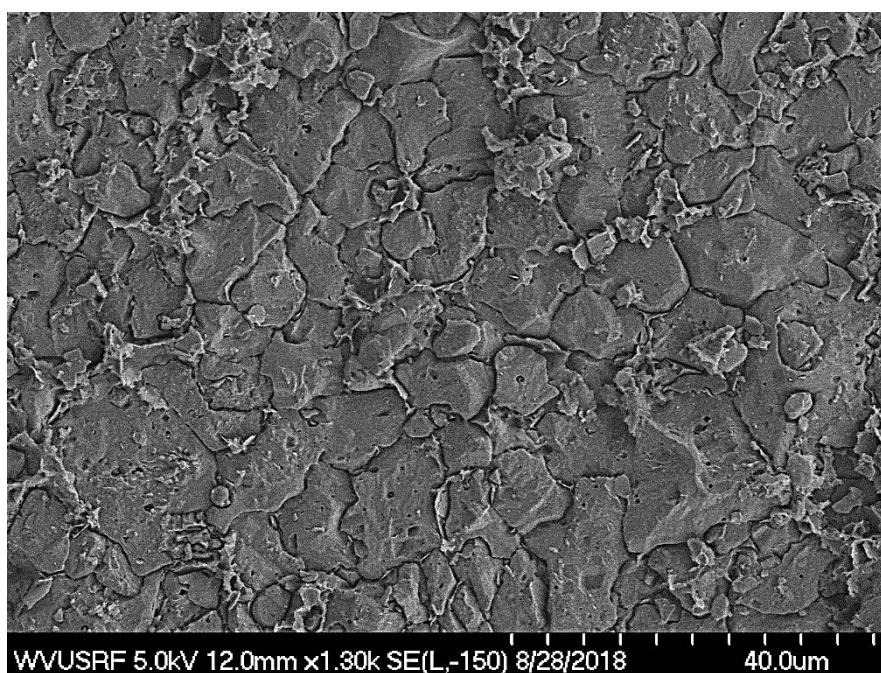
Figure 58. BSE SEM image of shale using 0.2M HCl for 1 minute

0.1 M HNO_3 was also used to observe the variation in the results. However, HNO_3 is a strong acid and it easily destroyed the specimen surface. In addition, there was a large number of authigenic minerals deposited on the surface which made it difficult to visualize

the grain boundaries. A sample SE and BSE image etched with 0.1 M HNO_3 for 1 minute is shown in Figures 59 and 60 respectively.
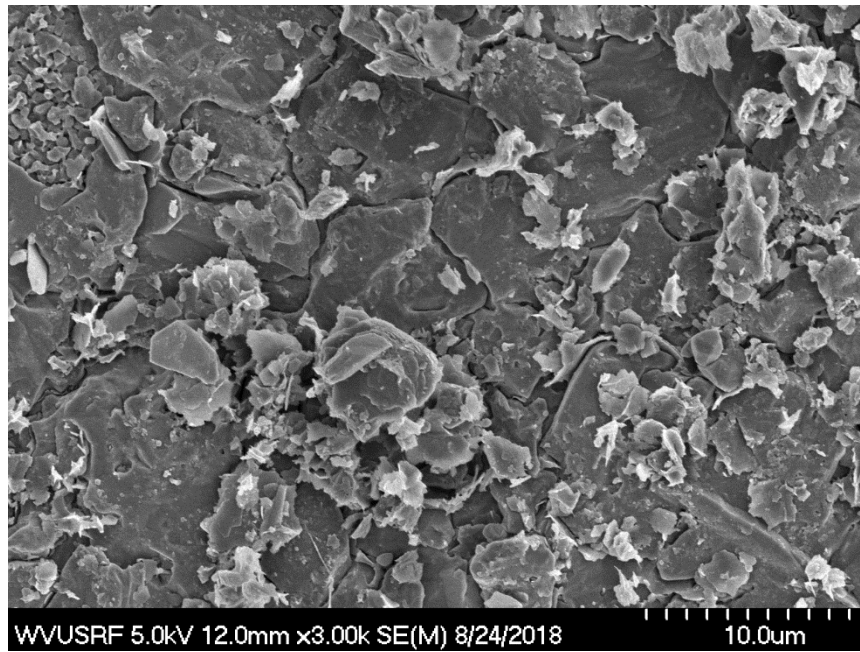
Figure 59. SE SEM image of shale using 0.1M HNO_3 for 1 minute
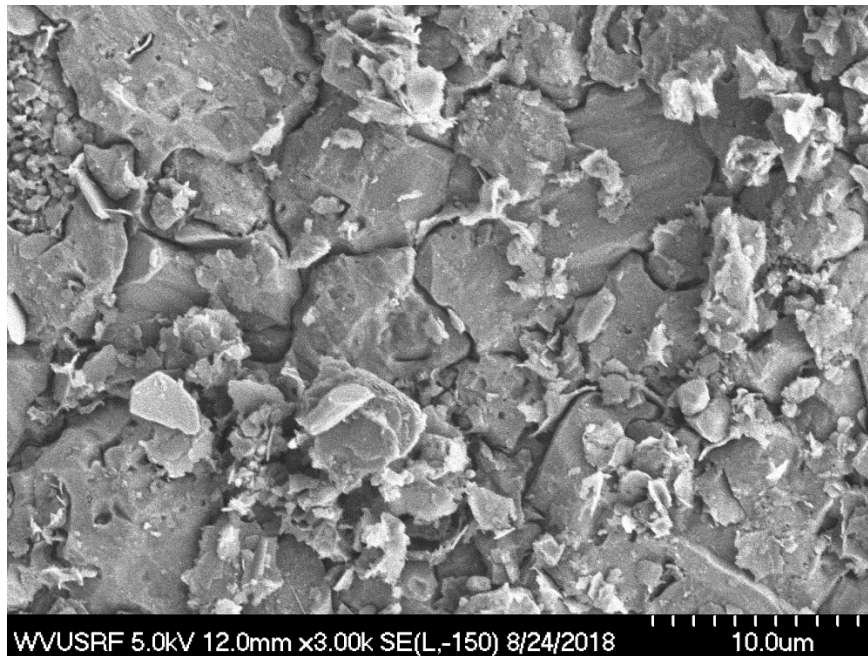
Figure 60. BSE SEM image of shale using 0.1M HNO_3 for 1 minute

Bibliography

Bajpayee, T., Pappas, D., & Ellenberger, J. (2014). What reportable noninjury roof falls in Underground Coal Mines Can tell us. *Prof Saf.*, Vol. 59(3). pp.57-62.

Barbour, T. G., Atkinson, R. H., & Ko, H. Y. (1979). Relationship of mechanical index and mineralogical properties of coal measure rock. *20th Symposium of Rock Mechanics*, (pp. 189-198). Austin, Texas.

Bazant, Z. P. (2005). *Scaling of structural strength 2nd edition.* Butterworth-Heinemann:Elseiver.

Bazant, Z. P., & Planas, J. (1998). *Fracture and size effect in concrete and other quasibrittle materials.* CRC Press LLC.

Bell, F. G. (1978). Physical and mechanical properties of the fell sandstones, Northumberland, England. *Engineering Geology*, 12(1), 1-29.

Bieniawski, Z. T. (1968). The effect of specimen size on compressive strength of coal. *International Journal of Rock Mechanics and Mining Sciences*, Vol 5, 325-335.

Bieniawski, Z. T. (1972). Propagation of brittle fracture in rock. *Proc. 10th Symp. on Rock Mechanics.* New York: AIMME.

Blanks, R. F., & McNamara, C. C. (1935). Mass concrete tests in large cylinders. *ACI*, Vol 31, issue 1, p 280-303.

Brindley, G. W. (1980). Quantitative analysis of clay mixtures. *Crystal Structures of clay minerals and their X-ray identification, Monograph 5 , Mineralogical Society, London*, pp. 411-438.

Clough, G. W., Sitar, N., & Bachus, R. C. (1981). Cemented sands under statis loading . *Journal of Geotechnical Engineering division*, 107(6), 799-817.

David, C., Menendez, B., & Bernabe, Y. (1998). The mechanical behavior of synthetic sandstoneswith varying brittle cement content . *International Journal of rock mechanics and mining sciences*, 35(6), 759-770.

Del viso, J. R., Carmona, J. R., & Ruiz, G. (2008). Shape and size effects on the compressive strength of high-strength concrete. *Cement and Concrete research 38*, 386-395.

Dobereiner, L., & De Freitas, M. H. (1986). Geotechnical properties of weak sandstone. *Geotechnique*, 36(1), 79-94.

Dube, A. K., & Singh, B. (1972). Effect of humidity on Tensile Strength of Sandstone. *Journal of Mines Metals and Fuel*, Vol.20, No.1, pp. 8-10.

Dutrow, B. L., & Clark, C. M. (2017). *X-Ray Powder diffraction (XRD)*. Retrieved from Integrating research and education: https://serc.carleton.edu/research_education/geochemsheets/techniques/XRD.html

Edet, A. (1992). Physical properties and indirect estimation of microfractures using Nigerian carbonate rocks as examples. *Engineering Geology*, 33, 71-80.

Ersoy, A., & Waller, M. D. (1995). Textural characterization of rocks. *Engineering geology*, vol. 39, pp. 123-136.

Evans, I., & Pomeroy, C. (1958). The strength of cubes of coal in uniaxial compression. In I. Evans, & C. Pomeroy, *Mechanical Properties of Non-Brittle Materials.* Butterworths Scientific Publications.

Fahy, M. P., & Guccione, M. J. (1979). Estimating strength of sandstone using petrographic thin-section data. *Bulletin of the Association of Engineering Geologists*, 16, 467-485.

Gaddy, F. L. (1956, August). A study of the ultimate strength of coal as related to the absolute size of cubical specimen tested. *Bulletin of the Virginia Polytechnic Institute*, pp. 1-27.

Gonnerman, H. F. (1925). Effect of size and shape of test specimens on compressive strength of concrete. *Proceedings ASTM* (pp. Vol.25 part II, p237). ASTM.

Gowariker, V. R., Viswanathan, N. V., & Sreedhar, J. (1986). *Polymer Science.* New Age International (P) Ltd.

Griffith, A. A. (1920). The phenomena of rupture and flaw in solids. *Phil. Trans. Royal Society of London.* London: Royal society of London.

Gunsalles, K. L., & Kulhaway, F. H. (1984). Comparative evaluation of rock strength measurements. *International Journal of rock mechanics and mining sciences and geomechanics abstracts*, 21(5),233-248.

Gyengo, T. (1938). Effect of type of test specimen and gradation of aggregate on compressive strength of concrete. *ACI J*, Vol 34, Issue 1, p. 269-284.

Hawkins, A., & McConnell, B. J. (1990). Influence of geology on geomechanical properties of sandstones. *7th International congress on Rock Mechanics*, (pp. 257-260). Achen.

Hodgson, K., & Cook, N. (1970). The effect of size and stress gradient on the strength of rock. *Proc. 2nd Congress of the Intl. Society for Rock Mechanics.* Belgrade.

Hoek, E., & Brown, E. T. (1980). *Underground excavations in rock.* London: Inst. Min. Metall.

Hoskins, J. R., & Horino, F. G. (1969). *Influence of spherical head size and specimen diameter of the uniaxial compressive strength of rocks.* U S Bureau of Mines Report of Investigations no. 7234.

Howarth, D. F., & Rowlands, J. C. (1986). Development of an index to quantify rock texture for qualitative assessment of intact rock properties. *Geotechnical Testing journal*, 169-179.

Howarth, D., & Rowlands, J. (1987). Quantitative assessment of rock texture and correlation with drillability and strength properties. *Rock Mechanics and Rock Engineering*, Vol 20, pp. 57-85.

Krinsley, D. H., Pye, K., JR., S. B., & Tovey, K. N. (1998). *Backscattered Scanning Electron Microscopy and Image Analysis of Sediments and Sedimentary Rocks.* Cambridge: Cambridge University Press.

MacGregor, J. G., & Bartlett, F. M. (1994). Effect of moisture condition on concrete core strengths. *ACI J*, Vol. 91, Issue 3, p. 227-236.

Malhotra, V. M. (1976). Are 4 multiplied by 8 inch concrete cylinders as good as 6 multiplied by 12 inch cylinders for quality control of concrete? *J Am Concr Inst*, Vol.73, Issue 1, p. 33-36.

Mark, C., Pappas, D. M., & Barczak, T. (2009). Current trends in reducing groundfall accidents in US coal mines. Littleton,CO: Society for Mining, Metallurgy and Exploration.

Medhurst, T. P., & Brown, E. T. (1998). A study of the mechanical behaviour of coal for pillar design. *International Journal of Rock Mechanics and Mining Sciences*, Vol.35, Issue 8, pp. 1087-1105.

Mogi, K. (1962). *The influence of the dimensions of the specimens on the fracture strength of rocks.* Tokyo: Bulletin of the Earthquake Research Institute, University of Tokyo.

Molinda, G. (2003). *Geologic hazards and roof stability in coal mines.* Pittsburgh,PA: Department of health and human services, Public health service, Centers for Disease Control and Prevention, National Institute for Occupational Health and Safety .

Molinda, G., & Mark, C. (n.d.). *Ground failure in coal mines with weak roof.* Pittsburgh: National Institute for Occupational Safety and Health.

Murphy, M. (2016). Shale Failure Mechanics and Intervention Measures in Underground Coal Mines: Results From 50 Years of Ground Control Safety Research. *Rock Mechanics and Rock Engineering*, Vol. 49(2): pp. 661-671.

Palchik, V. (1999). Influence of Porosity and Elastic Modulus on Uniaxial Compressive Strength in Soft Brittle Porous Sandstones. *Rock mechanics and Rock Engineering*, 32(4), 303-309.

Pappas, D. M., & Mark, C. (2009). *Roof and rib fall incident trends: a 10-year profile.* Pittsburgh, PA: National Institute for Occupational Safety and Health.

Phillipson, S. E. (2008). Texture, mineralogy and rock strength in horizontal stress-related coal mine roof falls. *International journal of Coal geology*, 175-184.

Pratt, H. R., Black, A. D., Brown, W. S., & Brace, W. F. (1972). The effect of specimen size on the mechanical properties of unjointed diorite. *International Journal of rock mechanics and mining sciences*, Vol 9.

Price, N. J. (1960). The compressive strength of coal measure rocks. *Colliery Engineering*, Vol.37, No.437, pp. 283-292.

Prikryl, R. (2001). Some microstructural aspects of strength variation in rocks. *International journal of rock mechanics and mining sciences*, 38, 671-682.

Rybacki, E., Reinicke, A., & Meier, T. (2015). What controls the mechanical properties of shale rocks?- Part I: Strength and Young's modulus. *Journal of Petroleum Science and Engineering*, Vol-135, pp. 702-722.

Shakoor, A., & Bonelli, R. E. (1991). Relationship between petrographic characteristics, engineering index properties and mechanical properties of selected sandstone. *Bulletin of the Association of engineering Geologists*, 28, 55-71.

Singh, S. K. (1988). Relationship among fatigue strength, mean grain size and compressive strength of a rock. *Rock Mechanics and Rock Engineering*, 21(4), 271-276.

Skelly, W. A., Wolgammot, J., & Vang, F.-D. (1977). Coal mine pillar strength and deformation prediction through laboratory sample testing. *18th US symposium on rock mechanics*, (pp. 2B5, 1-5). Golden, colorado.

Smart, B. D., Rowlands, N., & Isaac, A. K. (1982). Progress towards establishing relationships between the mineralogy and physical properties of coal measure rocks. *International Journal of rock mechanics and mining sciences and geomechanics*, 81-89.

Smordinov, M. I., Motovilov, E. A., & Volkov, V. A. (1970). Determination of correlation relationships between strength and some physical characterisctics of rocks. *Proceedings of the 2nd Congress of the International Society of Rock Mechanics*, (pp. pp. 35-37). Belgrade, Yugoslavia.

Spry, A. H. (1976). The comprehensive strength and texture of some Australian quartzites. *Australian Mineral Development Laboratories Bulletin* , pp. 21, 9-24.

Srodon, J., Drits, V. A., McCarty, D. K., Hsieh, J. C., & Eberl, D. D. (2001). Quantitative X-ray diffraction analysis of clay-bearing rocks from random preparations. *Clay and clay minerals*, Vol.49,No.6, 514-528.

Steart, F. A. (1954). Strength and stability of pillars in coal mines. *J. Chem. Metall. Min. Soc. S. Afr.*, Vol 54, 309-325.

Swapp, S. (2017, May 26). *Scanning Electron Microscopy (SEM)*. Retrieved from Integrating Research and Education: https://serc.carleton.edu/research_education/geochemsheets/techniques/SEM.html

Taylor, J. M. (1950). Pore-space reduction in sandstones. *Bulletin of the American Association of Petroleum Geologists*, 34, 701-716.

Tokyay, M., & Ozdemir, M. (1997). Specimen shape and size effect on the compressive strength of higher strength concrete. *Cement and Concrete Research*, Vol.27, No.8, pp. 1281-1289.

Tugrul, A., & Zarif, I. H. (1999). Correlation of mineralogical and textural characteristics with engineering properties of selected granitic rocks from Turkey. *Engineering geology*, 51, 303-317.

Ulusay, R., Tureli, K., & Ider, M. H. (1999). Prediction of engineering properties of a selected litharenite sandstone from its petrogrpahic characteristics using correlation and multivariate statistical techniques. *Engineering geology*, 51, 303-317.

Vutukuri, V. S., Lama, R. D., & Saluja, S. S. (1974). *Handbook on mechanical properties of rocks* .